SAND2022-1224J

# Introduction to Spectral Line Shape Theory

**T. A. Gomez[1], T. Nagayama[1], P. B. Cho[2], D. P. Kilcrease[3], C. J. Fontes[3], M. C. Zammit[3]**

[1]Sandia National Laboratories, Albuquerque, New Mexico 87123, USA
[2] University of Texas, Austin, Texas 78712, USA
[3] Los Alamos National Laboratory, Los Alamos, New Mexico 87545, USA

**Abstract.** Spectral line-shape models are an important part of understanding high-energy-density (HED) plasmas. Models are needed for calculating opacity of materials and can serve as diagnostics for astrophysical and laboratory plasmas. However, much of the literature on line shapes is directed toward specialists. This perspective makes it difficult for non-specialists to enter the field. We have two broad goals with this topical review. First, we aim to give information so that others in HED physics may better understand the current field. This first goal may help guide future experiments to test different aspects of the theory. Second, we provide an introduction for those who might be interested in line-shape theory, and enough materials to be able to navigate the field and the literature. We give a high-level overview of line broadening process, as well as dive into the formalism, available methods, and approximations.

**Contents**

**1 Introduction** **3**

**2 Conceptual Picture for Spectral Lines and Broadening** **5**
2.1 Bound-Bound Transitions . . . . . 5
2.2 Natural Broadening . . . . . 6
2.3 Plasma Broadening . . . . . 7

**3 Key Ingredients for Line-Shape Calculations** **8**
3.1 Ingredient 1: Interaction Between Atom and Plasma . . . . . 8
3.2 Ingredient 2: Atomic Structure for Isolated Atom . . . . . 9
3.3 Ingredient 3: Plasma Particle Motion In the Vicinity of the Radiator . 10
3.4 Ingredient 4: Ensemble Average of Random Perturbations . . . . . 11

**4 Line-Shape Formula and Various Approaches** **12**
4.1 Simulation Method . . . . . 14
4.1.1 Simulation Details . . . . . 14
4.1.2 Integration of Time-Dependent Schrödinger Equation . . . . . 15
4.1.3 Spectrum Generation . . . . . 16
4.2 Semi-Analytic Methods . . . . . 16
4.2.1 The Impact, Relaxation and Kinetic Theories . . . . . 18
4.2.2 Expressions for $\langle M(\omega)\rangle_e$ . . . . . 20
4.2.3 Additional Comments about the Impact, Relaxation, and Kinetic Theories . . . . . 21
4.2.4 Properties of the $\langle M(\omega)\rangle_e$ . . . . . 22

**5 Common Approximations and their Validity** **22**
5.1 The Electric Dipole Approximation . . . . . 23
5.2 Factorization of the Density Matrix . . . . . 25
5.3 Screening Approximations . . . . . 27
5.4 Classical Approximation . . . . . 29
5.5 Static-Ion Approximation . . . . . 31
5.6 Second-Order Approximation . . . . . 31
5.7 Binary-Collision Approximation . . . . . 34
5.8 Impact Approximation . . . . . 34
5.9 The Approximations used by Different Methods . . . . . 35

**6 Future Outlook** **38**

**7 Acknowledgements** **38**

**A Derivation of the Fundamental Line-Shape Formula** **40**

**B On the Liouville Notation** **41**

**C The $T$-matrix and the Lippmann-Schwinger Equation 42**
C.1 The Green's function . . . . . 44
C.1.1 Adding a Term to Remove the Singularity . . . . . 45
C.1.2 Strategic Placement of Quadrature Points . . . . . 46
C.1.3 Performing the p.v. integral inside a Quadrature rule . . . . . 46
C.1.4 Bilinear form of Green's function . . . . . 47
C.2 Some useful Relationships: "Reactance" $K$-matrix and "Scattering" $S$-matrix . . . . . 47
C.3 Relationship of $E$ to the state vectors: On-Shell and Off-Shell $T$-matrices 48

**D The $M$-operator and the Collision $T$-matrix 48**

## 1. Introduction

Spectroscopy is one of the best tools that we have to study the properties of laboratory plasmas and astrophysical objects such as stars. From the analysis of spectra, one can determine the velocity or rotation of an object, as well as that object's temperature, density, composition, or if it has magnetic fields. The shapes of spectral lines are sensitive to the density and temperature of the plasma. A dense plasma will cause spectral lines to shift and broaden. To understand spectra coming from dense plasmas, we need to model how the line shape changes as because of its plasma environment.

Line-shape models are essential for many high-energy-density (HED) physics applications, including plasma diagnostics and opacity calculations. Least-squares fitting of line-shape models to data can help determine the conditions in the plasma. Flawed models can lead to inaccurate determination of plasma conditions. Another use for line-shape models is to calculate opacities, which are essential for radiation-hydrostatic/hydrodynamic simulations needed for modeling stellar structure and designing HED experiments. The broadening of spectral lines affects how radiation propagates through material. Broader spectral lines can increase the Rosseland mean opacity [1] and inhibit radiation transport.

Due to the wide range of applications, inaccuracies in line-shape models can have far-reaching consequences. For example, inaccurate models of hydrogen broadening can lead to incorrect mass determination of white dwarfs, which ultimately can affect the determination of stellar ages, and by extension, constraints on the age of the galaxy and the universe [2]. Also, uncertainties in Mg K-shell spectra obscure true data-model discrepancies in the Fe-opacity experiment [3, 4]. Additionally, opacities in stellar atmospheres and interiors may be underestimated due to inaccuracies in the broadening of the Ly$\alpha$ lines of hydrogen [5] and oxygen [6], respectively. Underestimates of the opacities can impact the accuracy of model spectra of stars and the location of the solar convection zone [7].

Spectral lines arise from bound-bound atomic transitions. They are shifted and broadened due to the perturbation of the plasma environment; this phenomenon is referred to as spectral line shape formation. When an atom in a plasma is absorbing or emitting a photon, it will simultaneously be perturbed by the plasma particles surrounding it. The broadening of spectral lines is the result of the ensemble average of all these perturbations. This broadening can modify the spectra in a non-trivial way, and these changes are sensitive to the plasma environment. Line-shape models can be useful for a number of applications, including diagnostics [61] and opacity modeling.

Atomic transitions are divided into bound-bound and bound-free transitions. The corresponding spectral features change depending on plasma conditions, and the changes become more severe as density increases. Changes in a spectrum are less sensitive to the temperature of the plasma. In low-density conditions, the atomic spectra will not deviate much from an isolated-atom description. But in high-density cases, spectral lines broaden so much that they have non-trivial line shapes. Additionally, the lines will become so broad that they merge into a continuum, thus shifting the bound-free continuum edge to lower energies. This effect is known as continuum lowering or ionization potential depression. These changes in the spectrum from low to high density are demonstrated in figure 1.

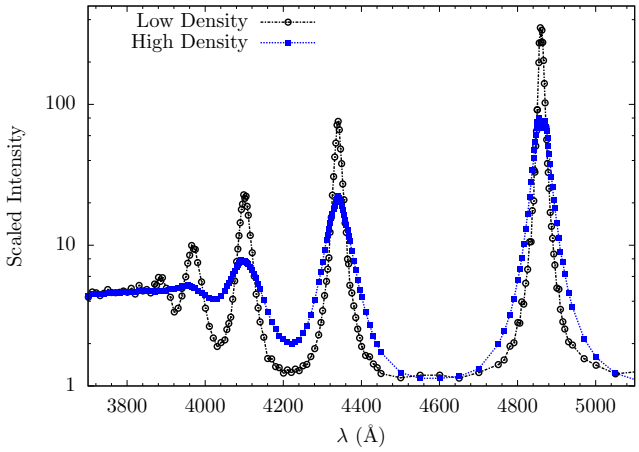


**Figure 1.** Measured spectra from Wiese *et al.* [8] data for low-density and high-density hydrogen. These spectra demonstrate empirically how the lines broaden with changing plasma conditions as well as merge into the continuum.

Unfortunately, accuracy of line-shape calculations is not known, as different models have different predicted shapes [9] and validating experiments [e.g., 8] are few and far between. One reason for this is that line shapes combine multiple fields of complex physics: atomic physics, plasma physics, statistical mechanics, and collisions. This leads to multiple approaches to the line shape problem, each using different approximations. Due to the different approaches, approximations, jargons, and notation, the literature is often inaccessible to non-specialists. This can create a barrier to entry into the field and make it difficult for non-specialists to understand the current state of line-shape calculations.

There are two goals of this paper. The first is to provide a broad overview of the theory of spectral line shapes for non-specialists. The second is to provide some introductory material for those who are wholly new to the field and wish to study line shapes. This paper approaches the line-shape problem from the point of view of fundamental physics, building conceptual understanding. We will also discuss the challenges associated with these calculations, and what approximations are commonly used to keep calculations tractable. Having a clear understanding of the field of line-shape theory allows us to more clearly understand the advantages and limitations of current calculations. We then take a critical look at the current status and recent progress in line-shape calculations and explore possible future directions.

One of the challenges faced by those new to spectral line-shape theory is navigating the wealth of literature. To aid in this task, we have presented the different theories using the same notation, so it is easier to see the true differences between them. Additionally, when trying to learn analytic line-shape theory, one needs to navigate not only the line-shape literature, but also the collision/scattering literature. We have, therefore, included an appendix giving a summary of scattering theory as it applies to spectral line shapes. While many of these details can be found in the literature, collating this information can be useful for those who are new to line shapes.

The rest of the paper is organized as follows. Section 2 gives a conceptual picture of line broadening. In Section 3, we discuss the key ingredients needed for line-broadening calculations. This discussion is intended to help the reader build a physical picture for the mechanisms behind line broadening, as well as illuminate the inter-disciplinary aspects and some of the challenges associated with line-shape calculations. Section 4 shows the fundamental equations for line shapes, and outline how the different approaches (simulation and semi-analytic) are used to tackle the problem. Section 5 contains a brief summary of the approximations commonly used in line-shape calculations. We end the paper by sharing recent progress in the field of line shapes and outline potential directions for the future. In the equations throughout we will use Hartree atomic units, and when we explore specific examples, the temperature of the plasmas we are exploring will be given in Kelvin or eV (1eV = 11,605K) and the densities will be given in $1/\text{cm}^3$. In this paper, we will not consider the effect of magnetic fields or the application to molecules in this document.

## 2. Conceptual Picture for Spectral Lines and Broadening

Spectral lines are the result of an atom transitioning between two bound states as a result of absorbing or emitting a photon. In a plasma, each radiator's energy levels are shifted—and they are shifted differently based on the surrounding environment. Since each radiator's energy levels are shifted differently, the average of all the spectra results in a broadening of the line as well as a net shift in energy or wavelength. In figure 2, we demonstrate this behavior with the Ly$\beta$ line of hydrogen. In the top panel, we have a schematic of a plasma, where the red, magenta, orange, and green points are radiators, and the blue points are perturbers. The spectrum produced by each of those radiators is plotted in the bottom panel, each with a different level of perturbation. Also shown in black is the ensemble average of all radiators; this is the observed spectrum.

In the rest of this section, we build intuition of line broadening. We briefly introduce what bound-bound transitions are, and how there is broadening of a line even in the absence of a plasma environment. We next build on this to introduce plasma line broadening.

### *2.1. Bound-Bound Transitions*

The structure and spectra of atoms without a plasma perturbation is fairly well understood. Atoms consist of a heavy positively charged nucleus with negatively charged electrons orbiting around it. How the electrons orbit around the nucleus depends on their energy. Those electrons with low energy will be bound to the atom, trapped in the attractive Coulomb well of the nucleus. And because the electrons are quantum particles, which behave as standing waves, the energies of the bound

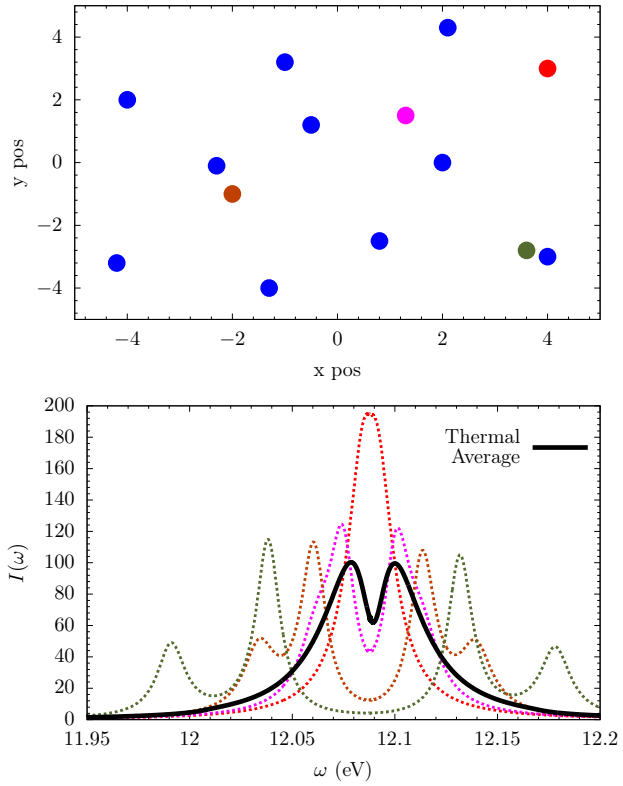


**Figure 2.** Top Panel: Cartoon of a plasma with red, magenta, orange, and green points indicating radiators, and blue dots representing perturbing plasma particles. Bottom Panel: The spectra of the H Ly$\beta$ line coming from perturbed radiators from the top panel. The color of each spectrum matches the color of each radiator in the top panel. Also shown is the observed line shape (black) which is a thermal/ensemble average of all perturbations. Here, $I(\omega)$ is the intensity in the spectra, and $\omega$ is the frequency of radiation.

electrons are discrete, meaning they can only occupy specific energies. The energy-level structure of electrons in atoms is explored extensively in textbooks such as [10, 11, 12].

The electrons bound to an atom interact with electro-magnetic radiation, i.e., photons, which can change the state of these electrons. If the energy of a photon is equal to the energy difference between two bound levels, then a transition can occur. Additionally, an electron can spontaneously decay from an upper state to a lower state and will emit a photon that has the energy of that transition. Transitions between two bound levels are referred to as bound-bound transitions. A schematic of the emission of radiation from an upper state, labelled $i$, to a lower state, labeled $j$, is shown in figure 3. There are other radiative processes, (e.g., bound-free), but because we are concerned with line broadening, we will not discuss them here.

### *2.2. Natural Broadening*

When an electron radiatively decays from an upper state, $i$, to a lower state, $j$, it will emit radiation at a frequency that is equal to the energy difference between the two

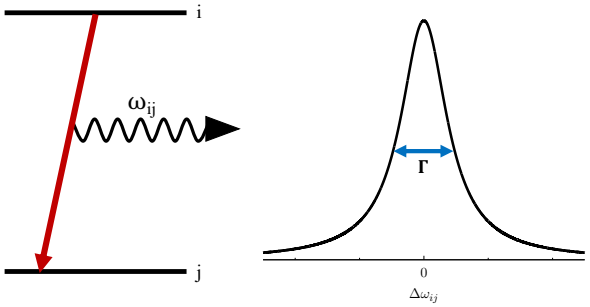


**Figure 3.** Cartoon of radiative decay from state $i$ to state $j$, and the corresponding Lorentzian line shape as a result of the natural decay rate of the radiation. Here, $\omega_{ij}$ is the frequency of radiation and $\Gamma$ is the width the spectral profile.

levels, $\omega_{ij} = E_i - E_j$. However, this spectral feature is not infinitely sharp, it has some width. There is a characteristic timescale for the electron to spontaneously decay from state $i$ to state $j$. This spontaneous decay is the result of vacuum fluctuations. The characteristic timescale for the decay from state $i$ to state $j$ is given by the Einstein $A$ coefficient (given in units of per second).

In a classical description of natural broadening, Heitler [13] demonstrates that if electrons from an excited state spontaneously decay, then that state has a finite lifetime. That finite lifetime translates to an uncertainty in the energy of the upper level (Heisenberg uncertainty principle)

$$\Delta E \Delta t \geq \hbar. \tag{2.1}$$

The uncertainty in energy, which we denote as $\Gamma$, is equal to the radiative decay rate (equal to $A$). This uncertainty in energy means that spectral lines are not infinitely sharp but have some finite width. The resulting spectral shape is a Lorentzian,

$$L(\omega) = \frac{1}{\pi} \frac{\frac{1}{2}\Gamma}{(\omega - \omega_{ij})^2 + \frac{1}{4}\Gamma^2}. \tag{2.2}$$

Demonstration of this line shape due to the spontaneous radiation process is shown in figure 3.

### *2.3. Plasma Broadening*

In a plasma, the atomic wavefunctions are perturbed and the energy levels are shifted due to perturbations from the nearby plasma particles, resulting in shifted lines during the emission and absorption processes. Neutral atoms, ionized atoms, plasma electrons can all perturb the radiating atom. For our purposes, we will focus on the charged particles, i.e., electrons and ions. Throughout this paper, we refer to the plasma ions and electrons as plasma particles or perturbers.

In low-density plasmas, the perturbation from the plasma is weak, meaning that energy-level shifts are small. In this limit, the plasma particles collide with the radiator, shortening the lifetimes of states $i$ and $j$. Therefore, the line shapes still

have a Lorentzian shape, but with a width that is a combination of the natural and collisional broadening. The atomic spectrum will then closely resemble that produced in the absence of a plasma.

However, as the density increases, the perturbation from the plasma becomes stronger, and the shifts in the atomic energy levels are larger. The larger shifts in energies mean that the line positions and widths will start to deviate from those produced for isolated atoms. The resulting line shapes become more complex than in the low-density limit.

While the broadening is an ensemble average of atomic structure under different perturbations, calculating atomic structure with an average perturbation will *not* result in broadening. There are some atomic-structure calculations that include the influence of the plasma in an average way such as average atom [14] or ion sphere [15, 16] models. These models produce bound-bound spectra that do not include any plasma broadening. Broadening of bound-bound transitions can only be achieved by averaging the spectra under the influence of individual perturbations and not by calculating the atomic structure with an average plasma potential.

## 3. Key Ingredients for Line-Shape Calculations

Line broadening is a multi-disciplinary field, requiring a combination of atomic physics, plasma physics, and statistical mechanics to perform calculations. Calculations of atomic structure and the perturbation requires knowledge of basic quantum mechanics, specifically atomic physics. The motion of the plasma particles around the atom affects the perturbations. Therefore, we need an understanding of plasma physics. Lastly, we need to perform an ensemble average, which requires an understanding of statistical mechanics. Each category (atomic physics, plasma physics, and statistical mechanics) has its own challenges. Taking elements of each and combining them adds additional complexity.

At their core, line-shape calculations perform a statistical average of perturbed atomic wavefunctions. Line-shape theory is based on performing a statistical average of solutions of the time-dependent Schrödinger equation,

$$\frac{d}{dt}\Psi(t) = [H_0^{(a)} + H_0^{(p)} + V(t)]\Psi(t) \tag{3.1}$$

where $H_0^a$ and $H_0^{(p)}$ are the Hamiltonians that describe the atom and plasma systems, respectively, and $V(t)$ is the interaction between atom and plasma. The 1$^{\text{st}}$ ingredient is an accurate description of the interaction between the atom and plasma particles, $V(t)$. The 2$^{\text{nd}}$ ingredient is a solution for the atomic wavefunctions and energies in the absence of plasma perturbation. The 3$^{\text{rd}}$ ingredient is a description of the wavefunctions/trajectories of the plasma particles. The last ingredient is how one performs the statistical/ensemble average of the $\Psi(t)$ solutions.

### *3.1. Ingredient 1: Interaction Between Atom and Plasma*

The first essential component is to accurately describe the interaction between the atom and the plasma particles. The components of the radiator—the nucleus and electrons—are charged particles, as are the plasma electrons and ions. Therefore, the interaction between the atom and plasma systems consists of a sum of Coulomb

interactions between particles,

$$V = \sum_i q_i \left[ \frac{Z_{\text{nuc}}}{|\vec{r}_i - \vec{r}_{\text{nuc}}|} - \sum_{a=1}^{N} \frac{1}{|\vec{r}_a - \vec{r}_i|} \right] + \sum_e q_e \left[ \frac{Z_{\text{nuc}}}{|\vec{r}_e - \vec{r}_{\text{nuc}}|} - \sum_{a=1}^{N} \frac{1}{|\vec{r}_a - \vec{r}_e|} \right], \quad (3.2)$$

where $q_i$ and $q_e$ are the charge of the ions and electrons, respectively, and $Z_{\text{nuc}}$ is the nuclear charge. Here, the first term in brackets is the interaction of the radiator with the ions and the second term is the interaction of the radiator with the plasma electrons. In quantum mechanics, the interaction between identical particles, such as two electrons or two protons, becomes more complicated due to an inability to distinguish them. Therefore, a more complete picture of the interaction between atomic and plasma particles includes what is called exchange terms, which accounts for the indistinguishability of identical particles [11]. This concept of indistinguishability is also tied to the Pauli exclusion principle, or Pauli repulsion.

In the line-shape problem, we are most concerned with the atom-plasma interaction. The plasma particles will also interact with each other. However, accounting for this interaction is complicated, and it is common to approximately account for the plasma particle-particle interactions by screening the atom-plasma interaction. A basic model for screening involves including an exponential damping factor to equation (3.2),

$$V_{scr} = \sum_i q_i \left[ \frac{Z_{\text{nuc}} e^{-|\vec{r}_i - \vec{r}_{\text{nuc}}|/\lambda_{scr}}}{|\vec{r}_i - \vec{r}_{\text{nuc}}|} - \sum_{a=1}^{N} \frac{e^{-|\vec{r}_a - \vec{r}_i|/\lambda_{scr}}}{|\vec{r}_a - \vec{r}_i|} \right] + \sum_e q_e \left[ \frac{Z_{\text{nuc}} e^{-|\vec{r}_e - \vec{r}_{\text{nuc}}|/\lambda_{scr}}}{|\vec{r}_e - \vec{r}_{\text{nuc}}|} - \sum_{a=1}^{N} \frac{e^{-|\vec{r}_a - \vec{r}_e|/\lambda_{scr}}}{|\vec{r}_a - \vec{r}_e|} \right]. \quad (3.3)$$

The use of screened interaction potentials was mathematically derived by Hussey *et al.* [17]. Screening $V$ has the effect of reducing the ability of more distant plasma particles to perturb the radiator.

### *3.2. Ingredient 2: Atomic Structure for Isolated Atom*

In order to use the form in equation (3.1), we first need to solve for the wavefunctions and energies of $H_0^{(a)}$. We need to solve the Schrödinger equation,

$$H_0^{(a)} \psi = E^a \psi \quad (3.4)$$

where $H_0^{(a)}$ is the Hamiltonian of the atomic system, $E^a$ is the energy of a given atomic state, and $\psi$ is the eigenvector/wavefunction solution associated with the energy $E^a$. Here, the Hamiltonian is given for an $N$-electron atom as

$$H_0^{(a)} = -\frac{1}{2}\nabla_{\text{nuc}}^2 + \sum_{a=1}^{N} \left[ -\frac{1}{2}\nabla_a^2 - \frac{Z_{\text{nuc}}}{|\vec{r}_a - \vec{r}_{\text{nuc}}|} + \sum_{a<a'} \frac{1}{|\vec{r}_a - \vec{r}_{a'}|} \right], \quad (3.5)$$

where the respective terms are the kinetic energy of the nucleus ($-\frac{1}{2}\nabla_{\text{nuc}}^2$), the kinetic energy of the electrons ($-\sum_a \frac{1}{2}\nabla_{\text{a}}^2$), the electron-nuclear potential energy

$(-\sum_a \frac{Z_{\rm nuc}}{|\vec{r}_a - \vec{r}_{\rm nuc}|})$, and the electron-electron Coulomb repulsion $(\sum_a \sum_{a<a'} \frac{1}{|\vec{r}_a - \vec{r}_{a'}|})$ ‡. Here, we have used the label $a$ to denote that these are atomic electrons. Due to the additional mass of the nucleus, the nucleus does not move much relative to the electrons. The most important contribution to the atomic structure is the relative motion of the electron to the nucleus,

$$H_0^{(a)} \approx \sum_{a=1}^{N} \left[ -\frac{1}{2}\nabla_a^2 - \frac{Z_{\rm nuc}}{|\vec{r}_a|} + \sum_{a<a'} \frac{1}{|\vec{r}_a - \vec{r}_{a'}|} \right], \tag{3.6}$$

where the nucleus is now taken to be the approximate center of mass frame.

As we can see from the form of equation (3.5), solving for atomic wavefunctions and energy levels is a complicated enough task all on its own. There are many codes that are devoted to solving the eigenvalue problem associated with equation (3.5), including Cowan's atomic structure code [12] (and its variant CATS [18]) the relativistic Dirac-Fock-Slater code RATS [19, 20], and the Flexible Atomic-structure Code (FAC) [21]. Cowan's code will usually produce adequate results using the Schrödinger equation with relativistic corrections, while RATS and FAC provide solutions of the Dirac equation.

### *3.3. Ingredient 3: Plasma Particle Motion In the Vicinity of the Radiator*

Next, we need to accurately describe the plasma behavior, by solving for the Hamiltonian of the plasma, $H_0^{(p)}$. The form is very similar to that of $H_0^{(a)}$,

$$H_0^{(p)} = -\sum_i \frac{1}{2}\nabla_i^2 + \sum_e \left[ -\frac{1}{2}\nabla_e^2 - \frac{Z_i}{|\vec{r}_e - \vec{r}_i|} + \sum_{e<e'} \frac{1}{|\vec{r}_e - \vec{r}_{e'}|} + \sum_{i<i'} \frac{Z_i Z_{i'}}{|\vec{r}_i - \vec{r}_{i'}|} \right], \tag{3.7}$$

where $i$ and $e$ denote ions and electrons, respectively, in the plasma.

As before, a simplified version is often used rather than equation (3.7). It is rare that all of the interaction terms (Coulomb potentials) between plasma particles are included in their solutions. Rather, only non-interaction terms (kinetic energy operators) between plasma particles are included in $H_0^{(p)}$, and the interacting terms are passed into $V(t)$ in the form of screening. The interactions between the atom and plasma particles become screened as already shown in equation (3.3).

It is common practice that the long-range potential of the atom is included in the solution for $H_0^{(p)}$. Here, "long-range" means outside the atomic orbitals. If the radiator is ionized, then we want to model the plasma particles being either attracted to, or repelled by, any bare nuclear charge $(Z_{\rm nuc} - N)$. This goal is achieved by splitting $V(t)$ into its long-range and short-range components,

$$V(t) = U_{long}(r) + V_{short}(t). \tag{3.8}$$

then use the long-range part $U_{long}(r)$ to alter the trajectories of the plasma particles in the vicinity of the atom,

$$H_0^{(p)} \approx -\sum_i \frac{1}{2}\nabla_i^2 + Z_i U_{long}(\vec{r}_i) + \sum_e -\frac{1}{2}\nabla_e^2 - U_{long}(\vec{r}_e), \tag{3.9}$$

‡ Here, we only show the non-relativistic version of the Schrödinger equation, relativistic corrections can be included [12], or one can solve the Dirac equation.

where $U_{long}$ usually takes the form of a Coulomb potential,

$$U_{long}(\vec{r}) = \frac{Z_{\text{nuc}} - N}{|\vec{r}|}. \tag{3.10}$$

The long-range atomic potential is important to describe the behavior of plasma particles near the radiator. If the radiator is neutral, meaning $U_{long}(r)$ is zero, then the particles move along plane-wave or straight-path trajectories. If the radiator has lost some electrons, then it has a net charge that will attract and accelerate electrons towards the radiator. Their behavior can be described by Coulomb waves (or hyperbolic trajectories). Additionally, with an attractive potential, the electrons may become (temporarily) bound when interacting with the radiator [22]. Because of the opposite charge, ions will be repelled from a positively-charged radiator.

### *3.4. Ingredient 4: Ensemble Average of Random Perturbations*

The last component we need is to perform a statistical average over atomic and plasma states, which requires a calculation of the probability that states of the atom and plasma are occupied. A derivation of the statistical average of quantum mechanical operators can be found in Fano [23], which we repeat that here.

Fano begins with a pure state, $\psi$, that is the only state available to the quantum system. The state $\psi$ is defined as a linear combination of states, $u_n$,

$$\psi = \sum_n c_n u_n. \tag{3.11}$$

where $u_n$ is some arbitrary set of wavefunctions and $c_n$ are the coefficients. A quantum-mechanical expectation value of an arbitrary operator, $O$, is given by

$$\langle O \rangle = \langle \psi | O | \psi \rangle . \tag{3.12}$$

Insertion of equation (3.11) into this definition for the expectation value gives a double sum over the $u_n$ states,

$$\langle O \rangle = \sum_{nn'} c^*_{n'} c_n \langle n' | O | n \rangle . \tag{3.13}$$

Let us now expand this concept where the wavefunction $\psi$ is made up of an ensemble of $\psi^{(i)}$. Each $\psi^{(i)}$ is associated with an ensemble statistical weight, $W_i$, where the sum of all weights equals unity,

$$\sum_i W_i = 1. \tag{3.14}$$

Here, the weight $W_i$ is the probability that $\psi^{(i)}$ is occupied in the ensemble. The expectation value becomes a sum over expectation values of $\psi^{(i)}$,

$$\langle O \rangle = \sum_i \langle O \rangle_i W_i. \tag{3.15}$$

$$\langle O \rangle_i = \left\langle \psi^{(i)} | O | \psi^{(i)} \right\rangle . \tag{3.16}$$

We can then use the notation in equation (3.13) to describe this non-pure state average,

$$\langle O \rangle = \sum_i \sum_{nn'} {c^{(i)}_{n'}}^* c^{(i)}_n W_i \langle n' | O | n \rangle . \tag{3.17}$$

We can therefore put all of the information on the statistical average into a single operator, which we call $\rho$,

$$\langle n|\rho|n'\rangle = \sum_i W_i c_{n'}^{(i)^*} c_n^{(i)}. \tag{3.18}$$

The operator $\rho$ is what is known as the density matrix. The density matrix gives us the probability that states are occupied in the ensemble. We can re-write the average in terms of the density matrix,

$$\langle O\rangle = \sum_{nn'} \langle n'|O|n\rangle \langle n|\rho|n'\rangle = \sum_{n'} \langle n'|O\rho|n'\rangle = Tr\{O\rho\}. \tag{3.19}$$

Here, we now have the general result that the statistical average of an operator is the trace of the product of that operator with the density matrix. The density matrix has to be properly normalized such that the trace is 1,

$$Tr\{\rho\} = 1. \tag{3.20}$$

In line-broadening theory, the form of the density matrix is often taken to correspond to a plasma that is in thermal equilibrium. Therefore, the density matrix is taken to be a Boltzmann distribution,

$$\rho = \frac{e^{-\beta H}}{Tr\ e^{-\beta H}}, \tag{3.21}$$

where $H$ is the Hamiltonian of the total atom and plasma system,

$$H = H_0^{(a)} + H_0^{(p)} + V \tag{3.22}$$

## 4. Line-Shape Formula and Various Approaches

Now that we have set up a conceptual picture for line broadening, we will now discuss methods of calculation. We begin with the rate for spontaneous emission,

$$A_{if} = \frac{\omega^3}{3c^3} |\langle i|\vec{D}|f\rangle|^2, \tag{4.1}$$

where $D$ is the electric dipole moment of the transition, and $i$ and $f$ indicate the initial and final states, respectively, of the transition. From this, we can derive the fundamental line-shape equation (see appendix A), given by [24, 25, 26, 27],

$$I(\omega) = \frac{\Re}{\pi} \int_0^\infty dt\ e^{i\omega t} Tr\left\{\vec{D}\cdot\vec{D}(t)\rho\right\}, \tag{4.2}$$

where $\Re$ means to take the real part. The line shape is then defined as the Laplace transform of the thermal-averaged dipole autocorrelation function. The dipole autocorrelation function (often denoted as $C(t)$),

$$C(t) = Tr\left\{\vec{D}\cdot\vec{D}(t)\rho\right\} \tag{4.3}$$

is a measure of the loss of coherence of the radiation due to the plasma environment. $C(t)$ decays to zero at long times. Calculation of the time evolution of the electric dipole moment is critical. There are two fundamental methods to evaluate equation

(4.2): analytic and simulation. We will expand on these two methods later in the section.

The time evolution of the dipole moment is evaluated in terms of time-evolution operators. According to the Heisenberg picture§, the time evolution of operators is written generally as

$$\vec{D}(t) = U^{\dagger}(t)\vec{D}U(t), \tag{4.4}$$

where $U(t)$ is a time-evolution operator. $U(t)$ is a unitary operator, meaning that

$$U^{\dagger}(t)U(t) = 1. \tag{4.5}$$

This condition guarantees that the sum of all probabilities is one, and particle number is conserved. The $U(t)$ operator can be obtained by integrating the time-dependent Schrödinger equation,

$$\frac{d}{dt}U(t) = -iH(t)U(t), \tag{4.6}$$

with the initial condition $U(0) = 1$. The time evolution of the dipole moment can equivalently be expressed in terms of Heisenberg's time evolution,

$$\frac{d}{dt}\vec{D}(t) = -i[H(t), \vec{D}(t)] \tag{4.7}$$

$$\frac{d}{dt}\vec{D}(t) = -iL(t)\vec{D}(t), \tag{4.8}$$

where the second equation is written with the compact Liouville representation (see appendix B). The Liouville representation is a compact way to write this commutation and lends itself to easy algebraic manipulation.

We demonstrate a few examples of the autocorrelation function and their corresponding line shapes in figure 4. In these plots, we have normalized the autocorrelation function so that $C(0) = 1$. The autocorrelation function has real and imaginary parts. The imaginary part is an indication of shifts or asymmetries. The autocorrelation function decays to zero at long times. Transitions such as H$\alpha$ ($n = 3 \rightarrow 2$)have a strong unshifted central component, with their autocorrelations decaying (roughly) exponentially. Transitions such as H$\beta$ ($n = 4 \rightarrow 2$) do not have a central component, and we see that the change of the real part from positive to negative leads to multiple peaks in the line profile.

We also need to discuss the relationship between frequency in the line shape and time in the autocorrelation function. This relationship is important because the time dependence of certain phenomena will impact different parts of the line shape. Time and frequency have inverse dimensions, with time usually defined in seconds, while frequency is defined inverse seconds. Therefore, processes that happen within a certain time $\Delta t$ will appear on the spectrum within a frequency range of $\Delta\omega = 1/\Delta t$. One example is the "static" limit in the wings of the lines: large $\Delta\omega$ corresponds to short $\Delta t$. At short $\Delta t$, the plasma particles do not move appreciably. Therefore, the particles are static within that given $\Delta t$ or $\Delta\omega$. Conversely, because small $\Delta\omega$ samples large $\Delta t$, the cores of lines are in the "dynamic" limit because plasma particles move appreciably within a large $\Delta t$.

§ There are three distinct pictures for time evolution in quantum mechanics. In the Schrödinger picture, the wavefunctions carry the time dependence, and operators are time independent. In the Heisenberg picture, the operators carry the time dependence, and the wavefunctions are time independent. In the interaction picture, time evolution is shared between wavefunctions and operators.

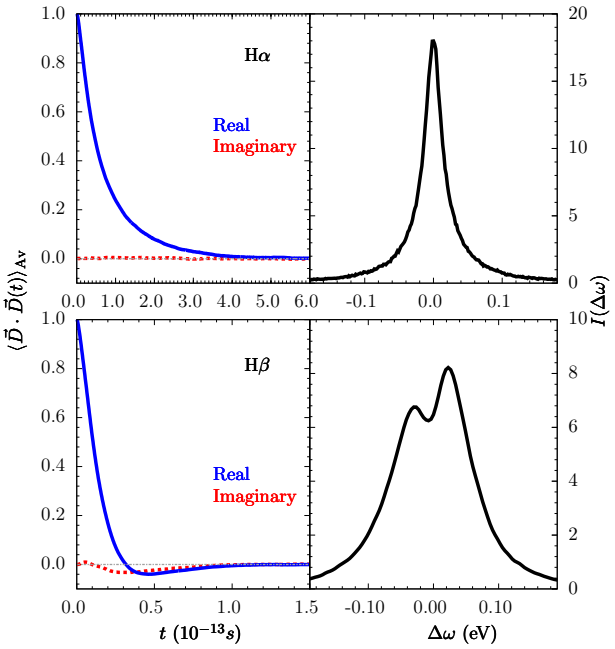


**Figure 4.** Examples of average $\vec{D} \cdot \vec{D}(t)$ and the corresponding line shapes for H$\alpha$ and H$\beta$. The blue lines indicate the real part of $\langle \vec{D} \cdot \vec{D}(t) \rangle_{Av}$, and dotted red indicates the imaginary part.

Line-broadening calculations are divided up into two broad categories: simulation and analytic methods. The simulation calculations simulate the plasma particles moving around the radiator to generate a perturbing potential, then numerically solve the time-dependent Schrödinger equation. The thermal average in simulations is usually done by simulating $\vec{D} \cdot \vec{D}(t)$ for many different radiators (i.e. Monte-Carlo sampling). Analytic methods involve the manipulation of equation (4.2) into a form that is convenient for computation. Simulations and analytic calculations approach the line-shape problem in different ways, and these methods are complementary. We now describe the details of each method.

### *4.1. Simulation Method*

Simulations are particularly convenient since they offer good insight into the line broadening problem. Plasma particles are simulated inside of a box, moving on classical trajectories. The classical particles are used to generate a time-dependent Coulomb potential $V(t)$. This time-dependent potential is used to solve for the time evolution of the radiator, which is then used to generate a spectrum. This procedure is outlined in figure 5, where this process is repeated for many different simulations with different initial conditions representing different radiators.

#### *4.1.1. Simulation Details*

The simulations vary in the details of their particle simulation. Generally,

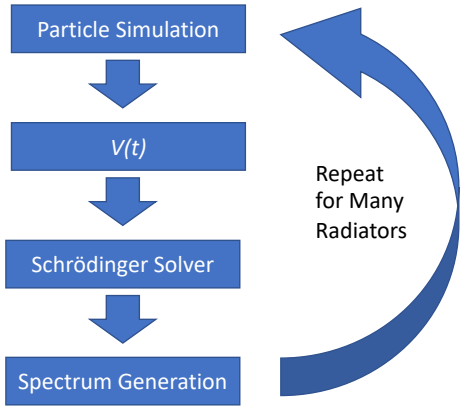


**Figure 5.** Conceptual outline of the simulation method of line broadening.

simulations will generate classical particles that move around in a finite-sized box. It is rare that a simulation will take into account all $N$-body interactions; Stambulchik *et al.* [28] and Gigosos *et al* [29] are exceptions. Rather, the simulation will generate particles that move on straight-path (neutral radiator) or hyperbolic (charged radiator) trajectories inside a finite-sized box. The lack of $N$-body dynamics can be mimicked by screening the atom-plasma interactions, equation (3.3).

The distribution of particle velocities and positions in the box are sampled from Maxwellian distributions. This generally involves random number sampling. One advantage of the non-interacting simulation is that the distribution of velocities remains Maxwellian. Therefore, for fully interacting simulations, care must be taken to avoid numerical heating or cooling [29].

To preserve particle numbers in the box, the simulation particles need to be re-injected back into the box. The re-injected particles need to preserve both the velocity distribution and the impact parameter distribution. Methods include periodic boundary conditions, mirrored walls [28], random sampling within an impact parameter bin [30], or completely re-sampling impact parameters and velocities [31].

### *4.1.2. Integration of Time-Dependent Schrödinger Equation*

Simulation methods will then take the time-dependent potential and solve for the time-evolution operator by numerically integrating the time-dependent Schrödinger equation. The challenge is to integrate

$$\frac{d}{dt}U(t) = -i[H_0 + V(t)]U(t), \tag{4.9}$$

where, as before $H_0$ contains the non-interacting terms, and $V(t)$ contains all the interacting terms. Because simulations approximate the plasma particles as classical, the $H_0$ in equation (4.9) spans only the atomic system, and $V(t)$ connects that atomic system to the plasma.

All simulation line-shape calculations are based on integrating equation (4.9), where the only variation would be in the simulation itself. At one of the Spectral

Line Shape in Plasma (SLSP) code-comparison workshops [32], all simulation codes were given the same $V(t)$ history, and the resulting $U(t)$ matrices were identical, independent of the integration method. Integration methods include implicit midpoint [33], explicit classic Runge-Kutta (RK4) with adaptive time steps [34], matrix exponential [35, 36], and Euler-Rodriguez parameters [30].

#### *4.1.3. Spectrum Generation*

The time-evolution operator that was obtained in equation (4.9) is then used to solve for the time evolution of the dipole moment:

$$\vec{D}(t) = U^{\dagger}(t)\vec{D}U(t).$$

This result is then used to calculate a spectrum in one of two ways. The first is by performing the Laplace transform of

$$Tr\left\{\vec{D}\cdot\vec{D}(t)\rho\right\}, \tag{4.10}$$

then averaging the various results. The second is to Laplace transform $\vec{D}(t)$ first (i.e. $\vec{D}(\omega)$), square it, then evaluate the thermal average,

$$Tr\{\vec{D}(\omega)\cdot\vec{D}(\omega)\rho\} \tag{4.11}$$

$$D(\omega) = \int_0^{\infty} dt e^{i\omega t} D(t), \tag{4.12}$$

and then average.

Analytically, these two methods are identical, but they have very different numerical robustness. Rosato *et al.* [37] showed that the power-spectrum method in equation (4.11) has substantially better noise properties than calculating the autocorrelation function in equation (4.10). The better noise properties of the power-spectrum method allow for much faster calculations because it will require fewer simulations. The noise of the two methods is demonstrated in figure 6 for the H$\beta$ transition of neutral hydrogen.

### *4.2. Semi-Analytic Methods*

Semi-analytic methods are used to solve equation (4.2) by relying on mathematical manipulation of equation (4.2), but still require a computer to perform the calculation of the line shape. Semi-analytic methods are advantageous over simulations because the computation time to calculate a line shape is generally much shorter and are without numerical noise. Additionally, since the derivations for analytic methods are different than the simulations, they can include different physics, but may also miss some physics that simulations include.

Since the work of Griem *et al.* [38], the contribution of the ions and electrons have been solved separately. Such a separation can be done because the ions and electrons have two drastically different velocities in the vicinity of the atom due to their masses. To account for the broadening due to the ions, the analytic method reduces the ion contribution to an integration over a plasma electric microfield. The method begins by assuming that the ions do not move appreciably over the decay time of $\left\langle\vec{D}\cdot\vec{D}(t)\right\rangle$, i.e. are static; see Section 5.5. The Hamiltonian used in the time evolution is modified

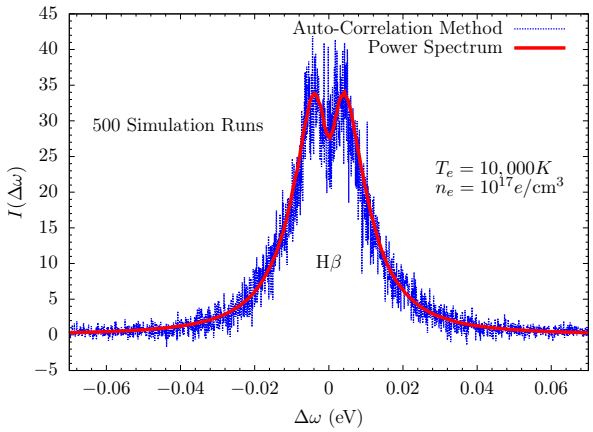


**Figure 6.** Demonstration of noise properties between equations (4.2) (blue) and (4.11) (red) for simulation calculations. Each calculation was performed with only 500 simulations. For the autocorrelation method to achieve the same level of noise as the power-spectrum method, the number of simulations needed would be in the tens of thousands.

accordingly,

$$\begin{aligned} H &= H_0^{(a)} + H_0^{(e)} + H_0^{(i)} + V^{(ea)} + V^{(ia)} \\ &\approx H_0^{(a)} + V_I^{(a)} + H_0^{(e)} + V^{(ea)} \\ &\approx H^{(ae)} \end{aligned} \quad (4.13)$$

where the superscripts $e$ and $i$ denote the plasma electrons and ions, respectively, and $V_I$ is the electric potential of the ions felt by the atom $a$. The atomic Hamiltonian now contains an external microfield (due to the ions) felt by the radiator atom $a$; we denote this simplified atom and plasma electron Hamiltonian as $H^{(ae)}$, which contains the potential due to the ions. The line-broadening equation is simplified to

$$I(\omega) = \frac{\Re}{\pi} \int_0^\infty dt\ e^{i\omega t} \times \left\langle Tr\left\{ \vec{D} \cdot e^{iH^{(ae)}t} \vec{D} e^{-iH^{(ae)}t} \rho \right\} \right\rangle_a . \quad (4.14)$$

where $\langle \rangle_a$ indicates an average of radiators, with each feeling different ion potentials; see figure 2.

To more conveniently average over different radiators feeling different ion potentials, the ion potential is approximated using the dipole interaction. Under the dipole approximation, the ion potential is defined to be the inner product of the dipole moment of the atom, $\vec{D}$, and the electric field of the ion, $\epsilon$, which is often referred to as the ion "microfield"; Section 5.1 gives more detail on the dipole approximation. The dipole approximation allows the average over radiators to be evaluated as an integral over ion electric fields, weighted by the microfield probability distribution. The microfield probability distribution gives the fraction of radiators that feel a given microfield. Calculation of microfield probability distributions is an entire area of research unto itself. The first calculations were performed by Griem *et al.* [38] and

were subsequently developed by Baranger & Mozer [39], Hooper [40], and Tighe & Hooper[41]. The most commonly-used calculation today is the APEX model [42], but can also be calculated by Monte-Carlo or molecular dynamics methods. The ion contribution is taken into account by integrating over the ion microfield probability distribution, $P(\epsilon)$. The line-shape equation is subsequently modified to be [38],

$$I(\omega) = \int_0^\infty d\epsilon P(\epsilon) J(\epsilon, \omega), \tag{4.15}$$

where $J(\epsilon, \omega)$ now contains the broadening due to the electrons. Ion-dynamics corrections are possible through models such as BID [43].

Next, we need to calculate the electron-broadening contribution. A convenient form for $J(\epsilon, \omega)$ involves algebraic manipulation of the time-evolution operators. First, the time evolution is written in terms of Liouville operators,

$$\begin{aligned} Tr\left\{\vec{D}e^{iH(\epsilon)t}\vec{D}e^{iH(\epsilon)t}\rho\right\} &= Tr\left\{\vec{D}e^{-iH(\epsilon)t}\rho\vec{D}e^{iH(\epsilon)t}\right\} \\ &= Tr\left\{\vec{D}e^{-iL(\epsilon)t}(\rho\vec{D})\right\}, \end{aligned} \tag{4.16}$$

where the order of the operators can be permuted due to the cyclic invariance of the trace; for compactness, we have dropped the superscript $(ae)$ from the Hamiltonians. The Liouville operators are convenient because they help to eliminate the plasma electron variables [26]. The electron-broadening function,

$$J(\epsilon, \omega) = \frac{1}{\pi}\Re \int_0^\infty dt\ e^{i\omega t} Tr\left\{\vec{D}e^{-iL(\epsilon)t}(\rho\vec{D})\right\}, \tag{4.17}$$

is manipulated so that all of the effects of the plasma electrons on the radiator are contained within a single operator,

$$J(\epsilon, \omega) = \frac{-1}{\pi}\Im Tr_a\left\{\vec{D}\frac{1}{\omega - L^{(a)}(\epsilon) - \langle M(\omega)\rangle_e}\rho_a\vec{D}\right\}, \tag{4.18}$$

where $\Im$ denotes taking the imaginary part, $L^{(a)}(\epsilon)$ is the Liouville operator of the atom, $\rho_a$ is the density matrix of the atom, and $\langle M(\omega)\rangle_e$ is the electron-broadening operator. The trace in equation (4.18) acts only on atomic variables, whereas the trace in equation (4.17) acts on both atomic and plasma electron variables. In the literature, there are multiple different representations of $\langle M(\omega)\rangle_e$, including $i\phi$, $\mathcal{H}$, $\langle M_c(\omega)\rangle$, $M(\omega)$, and $\mathcal{H}(\omega)$. There are three primary derivations for $\langle M(\omega)\rangle_e$: impact, relaxation, and kinetic. We discuss these theories later in this section.

In summary, analytic theory involves separate calculation of electron and ion broadening. At a given ion microfield, we need to calculate the electron broadening at that field value, which is used to calculate a spectrum, then average over the microfields felt by different radiators. This process is outlined in figure 7.

### *4.2.1. The Impact, Relaxation and Kinetic Theories*

The impact theories of Baranger [44] and Kolb & Griem [45] were the first broadly used models for plasma physics and astrophysical applications. The impact-theory results require multiple approximations, including using a simplified density matrix and the impact approximation. Additionally, it was Baranger's insight to interpret

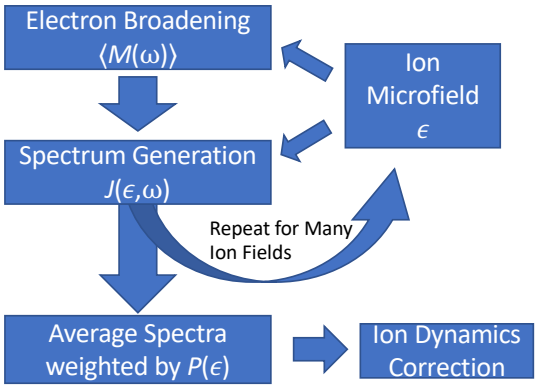


**Figure 7.** Conceptual outline of the analytic method of line broadening.

the broadening due to electrons with the same mathematical language as natural broadening.

The most important approximation to consider is the impact approximation, which allows for a significant simplification of Baranger's [44] results. Here, Baranger was only concerned with time evolution longer than some characteristic collision time scale, $\tau$. By looking at long times, the resulting $\langle M(\omega)\rangle$ will be independent of $\omega$ and the line shape will have a Lorentzian shape. This approximation is only valid as long as

$$\Im \langle M \rangle_e \tau \ll 1 \tag{4.19}$$

$$\Re \langle M \rangle_e \tau \ll 1. \tag{4.20}$$

Fano [26] sought to re-derive Baranger's results with more generality using the Liouville representation; this became the basis of the relaxation theory. The Liouville representation lent itself to easier mathematical manipulation and allowed Fano to remove the plasma electron variables more easily. With the Liouville representation, Fano [26] was able to include previously neglected terms in the broadening, specifically the time-/frequency-dependence of the electron collisions. Fano's result provided an extension of Lippmann & Schwinger's [46] collision theory into the Liouville representation. An overview of collision physics is presented in Appendix C. Lastly, Fano showed that his results reduced to Baranger's in the appropriate limit.

Fano's derivation, however, still relied on a simplified density matrix, and the formalism did not lend itself to easy inclusion of $N$-body physics. Fano (and Baranger) justified the use of the simplified density matrix by showing that the neglected parts would only be important in the far line wings. Additionally, Fano showed how $\langle M(\omega)\rangle$ might include $N$-body effects with a gas-density expansion, with even the $n_e^2$ term being complicated. It had been realized quickly that some of these $N$-body effects have a significant impact on the line shape [47]. So, while screening must be included for accurate line shapes (see Section 5.3), the screening prescriptions are ad hoc inclusions into the theory based on intuition rather than any rigorous derivation [38, 48].

Due to the calculational challenges associated with line-shape theory, Hussey *et al.* [17] sought to simplify the $N$-body problem into a few-body problem using non-

equilibrium statistical mechanics. Hussey *et al.* [17] used the Bogoliubov-Born-Green-Kirkwood-Yvon (BBGKY) [49, 50, 51, 52] hierarchy of kinetic equations to derive $\langle M(\omega)\rangle$. Within this formalism, Hussey *et al.* [17] were able to derive a line shape that includes a more general treatment of the density matrix and includes a formal treatment of screening. The kinetic theory formally includes terms that contain 3- or 4-body interactions, but this form is still challenging. These terms are too difficult to implement in current line-shape calculations.

### *4.2.2. Expressions for* $\langle M(\omega)\rangle_e$

Here, we will give the expressions for $\langle M(\omega)\rangle_e$ as derived by the impact, relaxation, and kinetic theories. This comparison will put all of the theories in the same notation so that their differences can be more clearly discerned. Both the relaxation and kinetic theories have terms that include $N$-body contributions, but for the purpose of this comparison we will not include them explicitly, but merely allude to them. We begin by comparing the relaxation and kinetic results and discuss the impact theory results last.

In the relaxation theory, Fano derived an expression for $\langle M(\omega)\rangle_e$ that is expanded in powers of electron density, $n_e$. The first term contains all interactions with a single plasma electron, then multiplied by the electron density. The second term contains all 3-body interactions (two plasma electrons + atom), etc. The expression for the relaxation theory is then (showing only the first-order density term),

$$\langle M_{\rm rel}(\omega)\rangle = n_e Tr_1\left\{L_I^{(a1)}\frac{1}{1-(\omega-L_0^{(a1)})^{-1}L_I^{(a1)}}\rho_1\right\} + \mathcal{O}(n_e^2) \quad (4.21)$$

where $L_I^{(a1)}$ is the Liouville representation of the interaction between the atom, $a$, and one plasma electron, 1, $L_0^{(a1)}$ contains non-interacting Hamiltonian terms of the atom and one electron, and $\rho_1$ is the density matrix of a single free plasma electron. In equation (4.3) of Hussey *et al.* [17], $\langle M(\omega)\rangle_e$ is given by

$$\langle M_{\rm kin}(\omega)\rangle = n_e Tr_1\left\{L_I^{(a1)}\rho_{a1}\times \frac{1}{1-(\omega-L_0^{(a1)}-C_{a1}(\omega))^{-1}\mathfrak{L}_I^{(a1)}}\right\}, \quad (4.22)$$

where $C_{a1}(\omega)$ contains additional terms including those that contain the effects of 3- or 4-body collisions.

The impact-theory results can be obtained from the relaxation theory by selecting a specific frequency. The formula for the impact-theory width is given by

$$\langle\alpha\beta\,|\langle M_{\rm imp}\rangle|\,\alpha'\beta'\rangle \simeq \langle\alpha\beta\,|\langle M_{\rm rel}(\omega_{\alpha\beta})\rangle|\,\alpha'\beta'\rangle \simeq \langle\alpha\beta\,|\langle M_{\rm rel}(\omega_{\alpha'\beta'})\rangle|\,\alpha'\beta'\rangle \quad (4.23)$$

where $\omega_{\alpha,\beta}$ and $\omega_{\alpha'\beta'}$ are the frequencies of the $\alpha\to\beta$ and $\alpha'\to\beta'$ transitions, respectively.

*4.2.3. Additional Comments about the Impact, Relaxation, and Kinetic Theories*

The reader can see that the line width is related to the function

$$M(\omega) = L_I^{(a1)} \frac{1}{1 - (\omega - L_0^{(a1)})^{-1} L_I^{(a1)}}, \tag{4.24}$$

which is the Liouville-equivalent of the collision $T$-matrix; see appendix D. The $T$-matrix is formally a collision amplitude. $M(\omega)$ consists of elastic $T$-matrices of the upper state and lower state, plus various interference terms between them.

One incredible insight by Baranger [44] was the relationship between of the width and the lifetime of the state. Baranger used the optical theorem, which converts an elastic $T$-matrix into a sum over inelastic and elastic cross sections. This way, Baranger was able to relate the width/lifetime of the state to the collision cross sections and amplitudes,

$$\Im \langle M_{\text{imp}} \rangle = \left\langle \frac{1}{2} n_e v \big[ \sigma_u^{\text{inel}} + \sigma_l^{\text{inel}} + \int d\Omega |f_u(\Omega) - f_l(\Omega)|^2 \big] \right\rangle_{\text{Av}}, \tag{4.25}$$

where $v$ is the velocity of the colliding particles, the first two terms are total inelastic cross sections, the last term contains elastic collision amplitudes, and the subscripts $u$ and $l$ denote the upper and lower states, respectively. This form is particularly convenient because all that one needs to calculate a line shape is a set of collision cross sections and amplitudes. However, caution must be taken with this formulation because it does not translate to overlapping lines [25]. Additionally because this is the impact theory, this form does not capture any time/frequency dependence of the collisions.

The form in equation (4.25) helps to illustrate that the broadening contains upper-state broadening, lower-state broadening, and some interference between them. The inelastic parts in Baranger's formula will constructively add, and the remaining elastic part in the third term will cancel if $f_u(\Omega)$ and $f_l(\Omega)$ are equal. Fano offered more insight, stating that collision events in the upper and lower states are not mutually exclusive events, but rather interfere with each other.

The kinetic theory employs a more general density matrix, rather than factorizing it. Hussey *et al.* [17], therefore took advantage of commutation properties to derive the expression in the kinetic theory. We make this point because the density matrix is "inside" of $M(\omega)$,

$$M_{kin}(\omega) = L_I^{(a1)} \rho_{a1} \frac{1}{1 - (\omega - L_0^{(a1)} - C_{a1}(\omega))^{-1} L_I^{(a1)}}. \tag{4.26}$$

This result is only possible when the following condition is satisfied:

$$[H, \rho] = 0, \tag{4.27}$$

which means that the kinetic theory may only applicable when equation (4.27) is true. Gomez *et al.* [53] re-derived an expression for $\langle M(\omega) \rangle_e$ within the relaxation theory with a more general density matrix treatment.

*4.2.4. Properties of the* $\langle M(\omega)\rangle_e$

First, $\langle M(\omega)\rangle$ is a complex-valued operator, where the real part gives the shift parameter and the imaginary part gives the width parameter. This can be seen by taking a simple form of $\langle M(\omega)\rangle$, where we consider only the diagonal elements and make them independent of $\omega$,

$$\langle M(\omega)\rangle \Rightarrow \langle M\rangle_R + i\langle M\rangle_I .$$

If we use this definition for the broadening, then the electron profile becomes

$$\frac{-1}{\pi}\Im\frac{1}{\omega - L - \langle M\rangle_R + i\langle M\rangle_I} = \frac{\langle M\rangle_I}{\pi}\frac{1}{[\omega - L - \langle M\rangle_R]^2 + \langle M\rangle_I^2}, \quad (4.28)$$

where, in this limit, the electron-broadening profile is a Lorentzian. One can easily see how in this representation, electron broadening can be thought of as simply decreasing the lifetime of the transition, harkening back to natural broadening.

More generally, $\langle M(\omega)\rangle$ has a frequency dependence and has off-diagonal elements, which have substantial impact on the spectra. The frequency dependence indicates that the shift and width parameters in equation (4.28) are now a function of frequency,

$$\frac{\langle M(\omega)\rangle_I}{\pi}\frac{1}{[\omega - L - \langle M(\omega)\rangle_R]^2 + \langle M(\omega)\rangle_I^2}$$

The consequences of including/neglecting the frequency dependence is shown in figure 8. Lastly, off-diagonal elements make the final line shape a superposition of Lorentzians [25] with frequency-dependent widths and shifts. The differences between the frequency-dependent width and shift parameters are measurable [8].

## 5. Common Approximations and their Validity

Performing all of the physics that was described in Section 3 exactly is challenging, and approximations have to be made to keep the calculations tractable. However, many approximations are used without sufficient justification. Without rigorously studying the validity of these approximations, both mathematically and comparing line shapes with different levels of approximation, the true validity/uncertainties of calculations is unknown. Quantifying uncertainties in a given model is difficult because different models employ different approximations. In this section we will discuss the following approximations: the dipole approximation, the factorization of the density matrix, classical approximation, static-ion approximation, second-order approximation, binary-collision approximation, impact approximation, and the approximations in screening treatments.

Line shapes can be calculated using simulation or analytic methods, and each method requires its own set of approximations. Some approximations—dipole, factorization of density matrix, screening, and classical approximations—are used by both simulation and analytic calculations. The remaining approximations—static-ion, second-order, binary-collision, and impact approximations—are only used in analytic calculations.

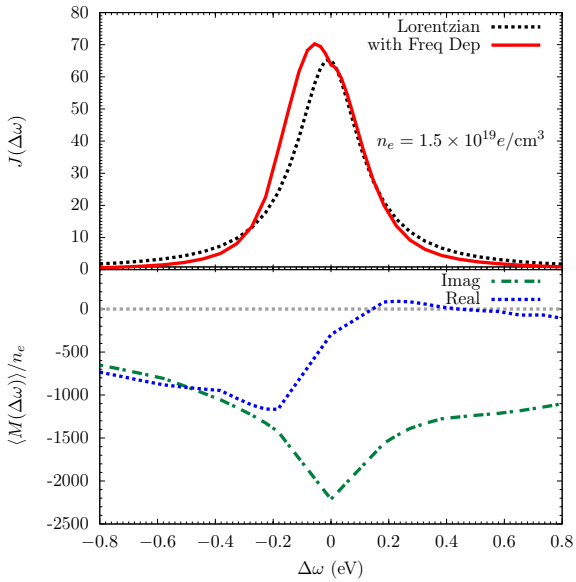


**Figure 8.** Bottom panel: frequency dependence of the $M$ operator. Dot-dashed green line is the imaginary part of $\langle M(\omega)\rangle_e$ and the dotted blue is the real part. Top panel: comparison of line shapes with frequency-dependent (red) and frequency-independent (dotted black) width and shift parameters. The frequency dependence puts the peak of the line shape in a different place, gives additional structure to the line shape, and depresses the wings of the lines.

### *5.1. The Electric Dipole Approximation*

The calculation of the Coulomb interaction between the radiator and the perturbers is fairly involved, and it is therefore desirable to simplify this interaction. Expanding the Coulomb interaction into its multipole components and retaining only the dipole component greatly simplifies the computational effort, and line shapes can be calculated using only electric fields. However, the dipole approximation is only valid when long-range interactions are the dominant type of interaction.

Since atomic electrons move in spherically symmetric potentials, the radial and angular wavefunctions are separated [54]. Therefore, it is advantageous to write the interaction in a spherical representation. The electron-electron repulsion term of equation (3.2) can be written in terms of spherical harmonics,

$$\frac{q_a q_e}{|\vec{r}_a - \vec{r}_e|} = \sum_{k=0}^{\infty} \frac{r_<^k}{r_>^{k+1}} P_k(\cos\gamma_{ae}) \tag{5.1}$$

$$= \sum_{k=0}^{\infty} \frac{r_<^k}{r_>^{k+1}} \sum_{q=-k}^{k} \frac{4\pi}{2k+1} Y_{kq}^*(\theta_a, \varphi_a) Y_{kq}(\theta_e, \varphi_e), \tag{5.2}$$

where $r_<$ and $r_>$ are the minimum and maximum, respectively, of $r_a$ and $r_e$; this expression is exact. The index $k$ can be thought of as the order of the multipole expansion, with $k = 0$ being the monopole interaction, $k = 1$ dipole, $k = 2$ quadrupole, and $k = 3$ octupole, etc.

Under the dipole approximation, we assume that the atomic electrons are always at the smaller radius, and the plasma electrons are always outside the wavefunction

of the atom. We therefore set

$$r_< = r_a \quad \text{and} \quad r_> = r_e \tag{5.3}$$

and use the Taylor expansion only up to the $k = 1$ dipole term. Under equation (5.3), the monopole, $k = 0$, electron-electron term cancels with the electron-nuclear term. The atom-plasma interaction is approximated as

$$\begin{aligned} V_{atom-plasma} \approx & \sum_i q_i \frac{r_a}{r_i^2} \sum_{q=-1}^{k} \frac{4\pi}{3} Y_{1q}^*(\theta_a, \varphi_a) Y_{1q}(\theta_i, \varphi_i) + \\ & \sum_e q_e \frac{r_a}{r_e^2} \sum_{q=-1}^{k} \frac{4\pi}{3} Y_{1q}^*(\theta_a, \varphi_a) Y_{1q}(\theta_e, \varphi_e) \\ \approx & \sum_{a=1}^{N} \vec{r}_a \left[ q_i \sum_i \frac{\vec{r}_i}{|\vec{r}_i|^3} + q_e \sum_e \frac{\vec{r}_e}{|\vec{r}_e|^3} \right] \qquad (5.4) \\ \approx & \sum_{a=1}^{N} \vec{r}_a \cdot \vec{\epsilon}_p \qquad (5.5) \\ \approx & -\vec{D}_a \cdot \vec{\epsilon}_p, \qquad (5.6) \end{aligned}$$

where $\vec{\epsilon}_p$ is the electric field due to the plasma, and $\vec{D}_a$ is the dipole moment of the atom.

The dipole approximation is particularly convenient because the plasma perturbation can be approximated as a fluctuating electric field, and atomic dipole moments of the atom can be obtained from any atomic structure code. As a result, this approximation is broadly used. Evaluation of the exact interaction (Eq 5.2) is more involved, requiring integrals over atomic wavefunctions, rather than just reading in a table of already calculated $\vec{D}_a$ values. Additionally, because plasma electrons and atomic electrons are identical, the Pauli exclusion principle should be applied to take into account their indistinguishability, which results in inclusion of exchange terms; the dipole approximation does not include this physics.

The dipole approximation gives rise to the term "Stark broadening". Equation (5.6) is the potential for the Stark effect. In most line-broadening scenarios, the dominant source of broadening will be through Stark interactions. Therefore, we can consider Stark broadening as a $1^{\text{st}}$-order effect of line broadening. There are other contributions to the broadening beyond the Stark effect, and exactly when it is important to include those other interactions depends on the element, transition, and the plasma conditions.

The dipole approximation is valid when the plasma particles are far away from the atom, because, even for $k = 1$, the true potential, equation 5.2, goes to some finite value rather than infinity as is the case in equation (5.4). This has already been explored by Woltz & Hooper [55], and we demonstrate it in figure 9. Due to this unphysical divergence, it is common practice (when using the dipole approximation) to employ some kind of cutoff, though not all calculations that use the dipole approximations have cutoffs [56]. The validity of these cutoffs has not been sufficiently studied, despite their having substantial impact on the line shape [9].

There have been a few studies that examined the consequences of not including the exact Coulomb interaction on the line shape. Expanding the dipole approximation to include quadrupole interactions may affect line asymmetries [35]. Not including the proper penetrative physics can lead to an overestimate of the true width [55]. And

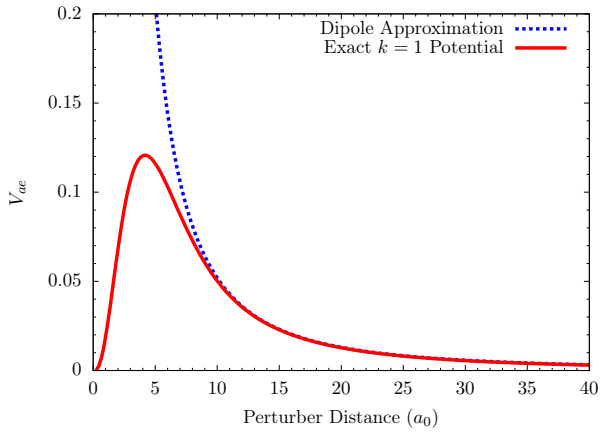


**Figure 9.** Comparison of the dipole approximation (dotted blue) with the exact $k = 1$ potential of equation (5.2), shown in red.

finally, when using the exact Coulomb interaction in equation (5.2), the monopole term, $k = 0$, does not cancel entirely with the nuclear term. The exact treatment of the $k = 0$ term leads to additional shifts not seen in the dipole approximation [57]. This shift occurs because the plasma electrons build up charge around the nucleus and screen it, thus lowering the energy of the atomic levels.

The redshift in the transition energies has been observed in experiments [58, 59, 60]. Additionally, this redshift has been recently used as an electron density diagnostic in a laser-heated solid-density Ti experiment [61]. In their work, including the redshift in the line-shape model allowed them to determine that the ions and electrons were not in equilibrium.

In figure 10, we show how accurate the dipole approximation is for two examples: neutral hydrogen, and He-like magnesium. For hydrogen Ly$\beta$ ($n = 3 \rightarrow 1$), the dipole approximation is sufficient to get the correct width of the line, but as supported by Gomez *et al.* [35], may be insufficient to capture the proper asymmetries. In Mg XI He$\gamma$ ($n = 4 \rightarrow 1$), the dipole approximation is not a good approximation. Here, the full-Coulomb treatment results in a smaller width as well as an additional redshift [57].

### *5.2. Factorization of the Density Matrix*

When the interaction between the atom and plasma is weak, the form of the density matrix in equation (3.21) can be simplified. The density matrix under Boltzmann statistics is given by

$$\rho = \frac{e^{-\beta H}}{Tr\ e^{-\beta H}} \tag{5.7}$$

where the Hamiltonian is that of the total atom+plasma system, given by

$$H = H_{atom} + H_{plasma} + V_{atom-plasma}. \tag{5.8}$$

If we assume that $V_{atom-plasma}$ is small, then we can neglect it in the evaluation

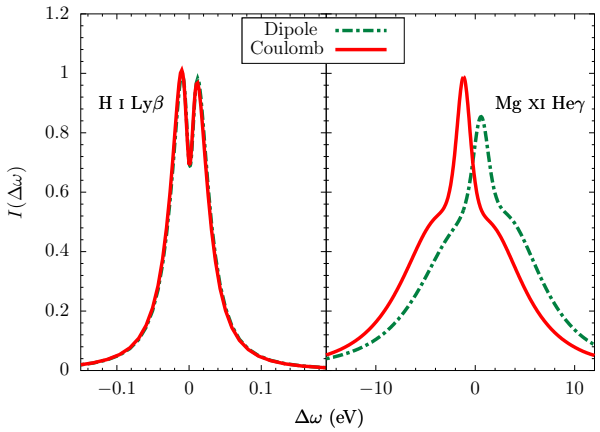


**Figure 10.** Comparison of the dipole approximation and full Coulomb interactions for neutral hydrogen and highly-ionized magnesium. In neutral hydrogen Ly$\beta$, the dipole approximation seems to be valid to get the correct width, but may be insufficient to get the proper asymmetry. In Mg XI He$\gamma$, the dipole approximation is not a valid approximation. The full Coulomb treatment results in smaller width. Additionally, the monopole term of the Coulomb interaction results in a redshift not captured by the dipole approximation.

of the density matrix. The density matrix can then be approximated as

$$\rho = \frac{e^{-\beta(H_{atom}+H_{plasma}+V_{atom-plasma})}}{Tre^{-\beta(H_{atom}+H_{plasma}+V_{atom-plasma})}} \tag{5.9}$$

$$\approx \frac{e^{-\beta(H_{atom}+H_{plasma})}}{Tre^{-\beta(H_{atom}+H_{plasma})}}. \tag{5.10}$$

Under this approximation, we can go further and factorize the density matrix into

$$\rho \approx \rho_{atom}\rho_{plasma} \tag{5.11}$$

$$\approx \left[\frac{e^{-\beta H_{atom}}}{Tre^{-\beta H_{atom}}}\right]\left[\frac{e^{-\beta H_{plasma}}}{Tre^{-\beta H_{plasma}}}\right]. \tag{5.12}$$

Factorization of the density matrix is possible because $H_{atom}$ and $H_{plasma}$ operate on separate variables and therefore commute. When two operators commute, they satisfy the following relationship:

$$[H_{atom}, H_{plasma}] = H_{atom}H_{plasma} - H_{plasma}H_{atom} = 0. \tag{5.13}$$

The interaction term, $V_{atom-plasma}$ does not commute with either $H_{atom}$ or $H_{plasma}$.

Omitting $V_{atom-plasma}$ from the density matrix ignores the possibility that the atom and plasma interaction can alter the distribution of states. In other words, the presence of the atom can alter the distribution of perturber states and vice versa. This effect is sometimes called a "back reaction". Neglecting the back reaction (i.e., neglecting $V_{atom-plasma}$) means that the atom and plasma are statistically independent, and has the advantage of using atomic energies and free plasma states to construct the density matrix.

The factorized-density-matrix approximation is valid in most cases. This approximation is justified analytically by Baranger [44] and Smith *et al.* [62], and numerically by Gomez *et al.* [53]. Baranger [44] and Smith *et al.* [62] showed that

the factorized density matrix, equation (5.11), gives an accurate line shape at the line center, but is erroneous in the wings. Differences between the factorized density matrix and a more complete density matrix treatment is indistinguishable at detunings (i.e. distance from line center) which are less than the temperature,

$$|\hbar\Delta\omega| < k_B T. \tag{5.14}$$

In Gomez *et al.* [53], using equation (5.9) resulted in a slight asymmetry not present in calculations using a factorized density matrix, and barely detectable except in the far line wings. Additionally, Griem *et al.* [63] showed analytically that calculations with a factorized density matrix [44] and a more complete density matrix [64] give the same shift. Therefore, if one is interested in line shapes at detunings less than the $k_B T$,

$$|\Delta\omega| \leq k_B T,$$

then the factorized density matrix is a good approximation, but if one is concerned with far-wing behavior, then one must consider the complete density matrix.

### *5.3. Screening Approximations*

In a plasma, the particles interact with each other, which causes the particles to rearrange themselves and can alter their motion in the plasma. Line-shape calculations can account for this behavior by using screened interactions. Solving for the full $N$-body dynamics is computationally expensive, and, to our knowledge, only Stambulchik *et al.* [28] and Gigosos *et al.* [29] have performed a line-shape calculation that fully considers the full $N$-body dynamics of a plasma with classical particles. It is much simpler to treat the plasma particles as non-interacting and make up for the missing correlations between them by screening the interactions between the atom and plasma particles. It is important to note that there has not been a rigorous formal derivation of screening in line-shape theory except within the kinetic theory [17]. Therefore, in all other instances where screening was used, it is out of intuition, and sometimes with an ad hoc treatment.

Even though the treatment of screening is often without derivation and ad hoc, it is still necessary to include it. Screening the atom-plasma interaction will reduce the strength of that interaction, making the line widths narrower than the unscreened case. This result has been well documented and is a critical part of calculating line shapes [38, 48]. Figure 11 shows how important screening can be to the line shape.

To include screening, one must modify equation (3.2) to include a screening factor,

$$\begin{aligned} V_{atom-plasma} = \sum_i q_i \Bigg[ & \frac{Z}{|\vec{r}_i - \vec{r}_{\rm nuc}|} e^{-|\vec{r}_i - \vec{r}_{\rm nuc}|/\lambda_{scr}} - \\ & \sum_{a=1}^{N} \frac{1}{|\vec{r}_a - \vec{r}_i|} e^{-|\vec{r}_a - \vec{r}_i|/\lambda_{scr}} \Bigg] \\ + \sum_e q_e \Bigg[ & \frac{Z}{|\vec{r}_e - \vec{r}_{\rm nuc}|} e^{-|\vec{r}_e - \vec{r}_{\rm nuc}|/\lambda_{scr}} - \\ & \sum_{a=1}^{N} \frac{1}{|\vec{r}_a - \vec{r}_e|} e^{-|\vec{r}_a - \vec{r}_e|/\lambda_{scr}} \Bigg]. \end{aligned} \tag{5.15}$$

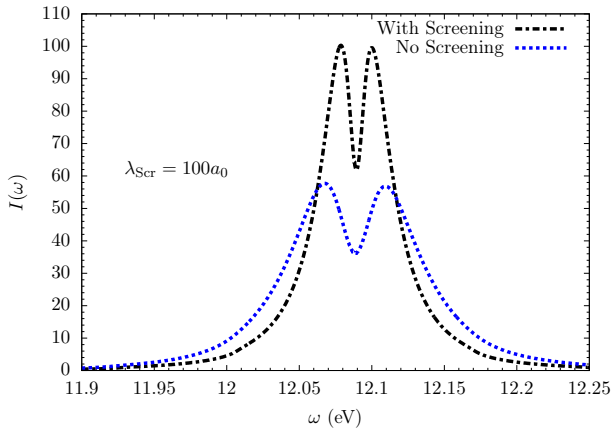


**Figure 11.** Comparison of Ly$\beta$ calculations with (dot-dashed black) and without (dotted blue) screening. Because screening weakens the interaction between atom and plasma, the line shape is narrowed.

The multipole expansion would likewise have to be modified. Equation (5.1) is modified accordingly:

$$\frac{1}{|\vec{r}_a - \vec{r}_e|} e^{-|\vec{r}_a - \vec{r}_e|/\lambda_{scr}} = - \frac{1}{\lambda_{scr}} \sum_{k=0}^{\infty} (2k+1) j_k \left( \frac{i r_<}{\lambda_{scr}} \right) h_k^{(1)} \left( \frac{i r_>}{\lambda_{scr}} \right) P_k(\cos\gamma), \quad (5.16)$$

where $j_k$ and $h_k^{(1)}$ are spherical Bessel functions, and spherical Hankel functions of the first kind, respectively. Under the dipole approximation, the screening modifies the formula for the atom-plasma interaction. The screened dipole interaction, equation (5.4), is then modified to be

$$V_{atom-plasma} \approx \sum_{a=1}^{N} \vec{r}_a \left[ q_i \sum_i \frac{\vec{r}_i}{|\vec{r}_i|^3} \left( 1 + \frac{|\vec{r}_i|}{\lambda_{scr}} \right) e^{-|\vec{r}_i|/\lambda_{scr}} + q_e \sum_e \frac{\vec{r}_e}{|\vec{r}_e|^3} \left( 1 + \frac{|\vec{r}_e|}{\lambda_{scr}} \right) e^{-|\vec{r}_e|/\lambda_{scr}} \right], \quad (5.17)$$

Iglesias [65] explores how the screening modifies the other multipole terms.

Line-shape calculations often use the Debye length,

$$\lambda_{\rm Debye} = \sqrt{\frac{\epsilon k_B T}{n_e}},$$

which is limited in accuracy; here $\epsilon$ is the vacuum permittivity. Debye screening is only valid for weakly coupled plasmas, and will break down at high density. The origin of Debye screening relies on a linearization of the Poisson-Boltzmann equation, meaning that it is only valid as long as the linearization approximation holds. Using a more accurate screening prescription would be highly desirable for calculating line shapes of strongly coupled plasmas.

*5.4. Classical Approximation*

It is common to approximate the plasma particles as classical point particles inducing fields around the radiator. This significantly reduces the size of the problem because $N$-body classical mechanics is a lot easier to solve than $N$-body quantum systems. The classical approximation therefore reduces the solution of a plane-wave state to a point-particle description with a definite position moving with a definite momentum,

$$e^{i\vec{k}\cdot\vec{r}+iEt} \Rightarrow \vec{r}(t) = \vec{r}_0 + \vec{k}t. \tag{5.18}$$

This classical approximation is only applied to the plasma particles, the radiator is still treated quantum mechanically.

With this simplification, instead of trying to solve for the total Hamiltonian as defined in equation (5.8), we can solve for the motion in pieces. We can solve for the motion of the classical particles using the laws of classical mechanics, and the perturbation of the radiator is obtained by integrating the time-dependent Schrödinger equation,

$$\frac{d}{dt}U(t) = -i\left[H_{atom} + V_{atom-plasma}(t)\right]U(t) \tag{5.19}$$

The Schrödinger equation solved in the quantum version is different than the classical version. In the quantum version, $U(t)$ contains both radiator and plasma time evolution, whereas in the classical case $U(t)$ contains only the radiator time evolution. In order to include the time-dependent behavior of the plasma in the time evolution of the atom, the interaction becomes a time-dependent operator. $V_{atom-plasma}(t)$ is now a time-dependent field that affects the atom.

This approximation ends up ignoring any potential quantum effects, such as the radiator and plasma electrons being indistinguishable (also known as exchange [11, 12]). It also ignores any changes in the shape due to the plasma electrons changing states, which includes the plasma electrons recombining during the radiation process [22].

The correspondence principle [66] can help determine the validity of the classical approximation. The correspondence principle states that, as the quantum numbers increase, the system will behave more like a classical system. For the plasma particles, the quantum numbers that define them are the momentum, both linear and angular. One indicator for the validity of the classical approximation is whether the thermal de Broglie wavelength,

$$\lambda_T = \sqrt{2\pi/mT}, \tag{5.20}$$

which is inversely dependent on the mass of the perturbing particle, $m$, and temperature, is small compared to the relevant length scales. Therefore, the higher the mass and the higher the temperature, the smaller the thermal de Broglie wavelength is and the more classical the plasma is. However, there is not a clear criterion for how small the thermal de Broglie wavelength has to be before we are in a classical or quantum regime. Smith *et al.* [62] outline some criteria for the validity of the classical approximation: 1) the wavepacket does not overlap with other wavepackets, 2) the wavepacket does not disperse or spread out over the course of the interactions, and 3) the atom-plasma potential does vary appreciably over the width of the wavepacket. One fairly strict condition that they give is that the thermal de Broglie wavelength must be much smaller than the typical particle spacing,

$$\lambda_T \ll n_e^{-1/3} \tag{5.21}$$

where $n_e$ is the electron density. If we insert equation (5.20) into equation (5.21), then the classical approximation is valid when $mT \ll n_e^{2/3}$. Smith *et al.* [62] also state that strong collisions may be a scenario where the classical approximation breaks down (more on this later). Whether to assume a classical or quantum mechanical description of electrons is not always clear, but ions, due to their increased mass, will always be in the classical regime.

In figure 12, we compare classical and quantum calculations for Ly$\alpha$ and Ly$\beta$ of hydrogen. At the lowest temperature, the quantum calculation gives a larger width than the classical calculation. We can only speculate for now that this is largely because the thermal de Broglie wavelength at $T_e$=10,000K is the roughly the same size as the $n = 2$ wavefunction. At the lowest temperature, $\lambda_T = 14a_0$, and the average distance between the electron and nucleus [equation (3.20) in 11],

$$|\vec{r}_e - \vec{r}_n|_{\rm Av} = \frac{1}{2Z}[3n^2 - l(l+1)].$$

is 6 $a_0$ for $n = 2$ of hydrogen. At 80,000K, the thermal de Broglie wavelength has shrunk to $4.98a_0$, which is smaller than the average electron extent. At this higher temperature, the plasma electrons are more classical, i.e., behaving more like a point particle, and we would expect the two calculations to come into agreement, which they do. If the hypothesis that

$$\lambda_T/|\vec{r}_e - \vec{r}_n|_{\rm Av} \lesssim 1 \tag{5.22}$$

must be satisfied in order for the classical approximation to be valid is correct, then we can test it by examining a different transition at the same temperature to see if this condition holds. In Ly$\beta$, the $n = 3$ wavefunction extent is $13.5a_0$, and at $T_e = 10,000$K it is on the cusp of satisfying equation (5.22), and we would expect that the discrepancy between classical and quantum to be less severe. In fact, the right panel of figure 12 shows that at $T_e = 10,000$K, the classical and quantum calculations predict nearly the same profile.

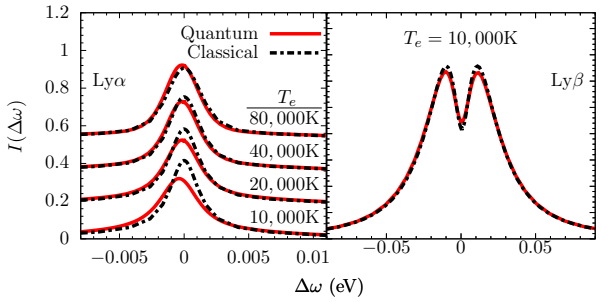


**Figure 12.** Comparison of quantum and classical calculations of the Ly$\alpha$ and Ly$\beta$ line. At 10,000K, $\lambda_T$ is larger than the average extent of the $n = 2$ (Ly$\alpha$) wavefunction. As temperature increases, $\lambda_T$ decreases and the electrons become more classical, and the two calculations come into agreement. $\lambda_T$ is of similar size as the $n = 3$ wavefunction, so we expect the difference between quantum and classical calculations to be much less. And indeed, that is what is seen for Ly$\beta$.

There is another aspect of electron collisions that is not well captured by classical calculations: electron capture. Electron capture is the phenomenon that occurs during

a collision with an atom when the plasma electron becomes temporarily bound to the atom. This phenomenon is also known as dielectronic capture and is the first step in the process of dielectronic recombination, which involves emission of a photon. Electron capture does *not* involve the emission of a photon.

Including electron capture has largely been neglected. Griem [27] predicted that this process should not contribute much to the line shape, and Alexiou & Ralchenko [67] showed that it was negligible for the application they studied. However, these studies did not explore the full parameter space. Our recent work [22] showed that for *some* transitions, the electron capture contribution could result in as much as a 100% increase in the line width. We found that electron capture was more important for lower-$n$ lines, and had more impact on the width when the atomic structure was highly non-degenerate, i.e., when $s$ and $p$ states had largely different energies for the same $n$. Our $2^{nd}$-order calculation showed that electron capture resolved the long-standing (factor of two) discrepancy between theory and experiment [68, 69, 70] for the B III $2s$-$2p$ transition.

### *5.5. Static-Ion Approximation*

We now begin the discussion of approximations that only apply to analytic calculations. In analytic calculations, the ion perturbers are assumed to be static over the relevant timescales. Because ions have substantially more mass than electrons, they travel through the plasma much more slowly than electrons. The motion of plasma ions is so slow that they can be considered not moving at all in the time that it takes $\left\langle \vec{D} \cdot \vec{D}(t) \right\rangle$ to decay. The big advantage of this assumption is that the ion perturbation can be simplified to an integration over a microfield distribution, and the focus then turns toward the details of electron broadening. The heavier the ion is, and the lower the temperature, the better this approximation is. And the converse is true, the static-ion approximation is worse with higher temperatures and lighter ions. For example, if a hydrogen radiator is in a hydrogen plasma, the ion dynamics corrections will be substantial, while if it were a trace element in, say, an argon plasma, then the corrections would be negligible.

The consequences of using this approximation are more pronounced in the core of the line rather than the wings. This behavior can be understood by thinking of different frequencies as sampling different timescales. Using a dimensional analysis argument, the detuning of the line, $\Delta\omega$, is inversely related to the time step $\Delta t$,

$$\Delta\omega = 1/\Delta t. \tag{5.23}$$

Therefore, we see that processes that take a long time to happen—such as the time it takes for ions to move appreciably—will affect the line at small $\Delta\omega$. And processes that happen on short timescales occur in the line wings. The wings are often referred to as the static limit because large $\Delta\omega$ corresponds to small $\Delta t$, where the ions do not move appreciably. The differences between static ion and dynamic ion treatments are shown in figure 13

### *5.6. Second-Order Approximation*

The second-order approximation is commonly used in analytic calculations. In analytic calculations, the derived formulae for line-broadening may be too complex/intractable, and simplifications can be made by Taylor expanding the formulae. Analytic theory

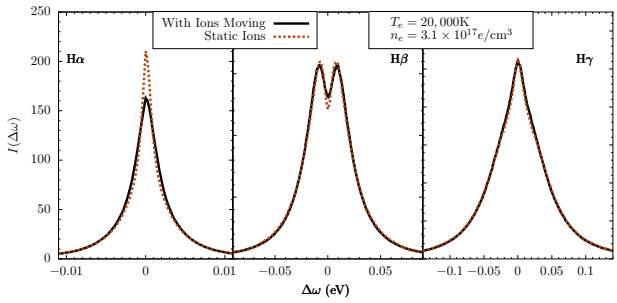


**Figure 13.** Demonstration of the validity range of the static ion approximation. The importance of ion dynamics decreases with increasing principal quantum number.

uses the $M(\omega)$ operator in equation (4.24) to define the width. For convenience, we repeat that formula here,

$$M(\omega) = \frac{1}{1 - L_I(\omega - L_0)^{-1}} L_I.$$

The inverse operator is difficult to evaluate, so it is Taylor expanded, using the expansion formula,

$$\frac{1}{1-x} = 1 + x + x^2 + \cdots. \tag{5.24}$$

This expansion formula is truncated at the second term, resulting in the approximate expression,

$$M(\omega) \approx \left[1 + L_I \frac{1}{\omega - L_0}\right] L_I. \tag{5.25}$$

The second-order approximation will break down when $L_I(\omega - L_0)^{-1}$ becomes large.

Fano [26] gives a physical interpretation of the validity condition for the $2^{nd}$-order approximation, relating it to memory effects. In irreversible thermodynamics, the notion of memory is that the behavior of the atom-plasma dynamics depends on its past behavior. When evaluating the product of

$$\left[L_I(\omega - L_0)^{-1}\right] L_I$$

one has to sum over a set of intermediate states,

$$\left[L_I(\omega - L_0)^{-1}\right] L_I = \sum_{a\mathbf{k}} \left[L_I(\omega - L_0)^{-1}\right] |a\mathbf{k}\rangle \langle a\mathbf{k}| L_I. \tag{5.26}$$

The operator $\left[L_I(\omega - L_0)^{-1}\right]$ will be small if the range of energies spanned by $a\mathbf{k}$ needed for the line shape is large. Large $\Delta E$ translates to large $\Delta\omega$, which, as we've discussed before, corresponds to short $\Delta t$. Fano states that this large span in frequency can be interpreted as the plasma having a short memory. Therefore, under this short-memory approximation, the broadening arises from the cumulation of weak and short collisions. Conversely, the breakdown of the $2^{nd}$-order approximation indicates that not only are the interactions stronger, but the collisions have a longer memory.

It is common to introduce strong-collision corrections when using the $2^{nd}$-order approximation, these corrections include cutoffs and adding constants. Strong collision cutoffs will omit certain processes from the broadening. For example, Griem *et al.* [38], rather than considering all plasma electron positions, only included plasma electron trajectories that were outside of a certain radius. Lee [71], instead of cutting off electron positions, cut off the momentum transfer, meaning that plasma electrons can only impart a maximum amount of momentum to the radiator. A constant was added back to account for the missing processes due to the cutoff procedure. Lastly, O'Brien & Hooper [56] used no cutoff whatsoever [9].

These strong collision cutoffs are not checked for validity. The strong-collision cutoffs are either theoretically motivated [38], ignored [56], or tailored to match other calculations [72]. The current procedures seem to do well when comparing against other calculations for hydrogen calculations [48]. For other scenarios, though, strong collision procedures need to be adjusted to match more accurate calculations [72].

The $2^{nd}$-order approximation could not be removed from analytic line-shape calculations until recently [73]. We were able to implement an all-order calculation for $M(\omega)$ by borrowing a technique from collision theory; the relationship between $M(\omega)$ and the collision T-matrix is given in appendix D. The $T$-matrix—formally a collision amplitude—is defined as (see appendix C)

$$T(E) = \frac{1}{1 - V[E - H_0]^{-1}} V,$$

where the parallels with $M(\omega)$ can be easily seen. The $T$-matrix solution can be obtained by re-arranging the problem, i.e.

$$[1 - V(E - H_0)^{-1}]T(E) = V. \tag{5.27}$$

If we write this expression with state vectors, then the $T$-matrix can be obtained as the solution of a set of linear equations,

$$\sum\!\!\!\!\!\!\int_{\alpha''\mathbf{k}''} \left\langle \alpha\mathbf{k} \right| [1 - V(E - H_0)^{-1}] \left| \alpha''\mathbf{k}'' \right\rangle \times \left\langle \alpha''\mathbf{k}'' \right| T(E) \left| \alpha'\mathbf{k}' \right\rangle = \left\langle \alpha\mathbf{k} \right| V \left| \alpha'\mathbf{k}' \right\rangle . \tag{5.28}$$

Here, $\sum\!\!\!\!\!\!\int_{\alpha''\mathbf{k}''}$ indicates a sum/integral over the atomic and plasma electron states. If this expression is discretized into a quadrature rule (where $W_{\alpha''\mathbf{k}''}$ represents an integration weight),

$$\sum_{\alpha''\mathbf{k}''} \left[ \delta_{\alpha\alpha''}\delta_{\mathbf{k}\mathbf{k}''} - V_{\alpha\mathbf{k},\alpha''\mathbf{k}''} W_{\alpha''\mathbf{k}''} \right] \times T_{\alpha''\mathbf{k}'',\alpha'\mathbf{k}'}(E) = V_{\alpha\mathbf{k},\alpha'\mathbf{k}'}, \tag{5.29}$$

then we can use linear-algebra $Ax = b$ solvers to obtain the $T$-matrix.

The impact of using all-order vs $2^{nd}$-order is not uniform across transitions and elements. Using all-order is more important for neutrals than it is for highly-ionized radiators. For highly-ionized radiators, the exposed nucleus accelerates plasma electrons in its vicinity, and their interactions with the bound electrons are therefore inherently weaker than for the neutral case. Additionally, highly-ionized radiators are more tightly bound to the radiator and are less polarizable, and their interactions with the plasma are ultimately weaker. In figure 14, we compare $2^{nd}$-order calculations to all-order calculations for Ly$\beta$ of neutral hydrogen and He$\gamma$ of $Mg^{11+}$.

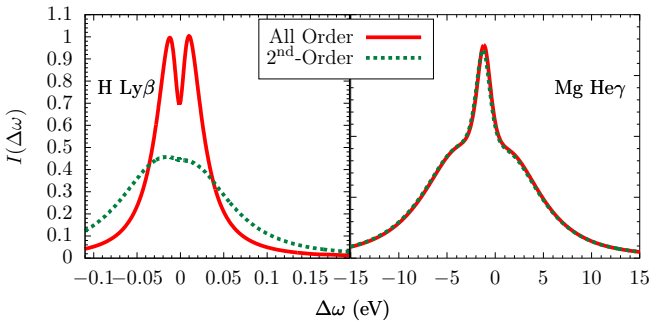


**Figure 14.** Comparison of all-order vs $2^{nd}$-order for neutral hydrogen and highly-ionized magnesium. $2^{nd}$-order method overestimates the line width of neutral hydrogen by at least a factor of two, while it closely approximates the all-order result for a highly-ionized radiator. The plasma conditions are $T_e$ = 0.9eV and $n_e = 10^{18} e/\text{cm}^3$ for the hydrogen plasma, and are $T_e$ = 180eV and $n_e = 3 \times 10^{22} e/\text{cm}^3$ for the magnesium plasma in a 50/50 mixture with iron.

### *5.7. Binary-Collision Approximation*

The binary collision approximation only considers two-body interactions between the atom and plasma electrons, and applies only to analytic calculations of electron broadening. In this approximation, the calculation focuses on the details of how the atom is perturbed by a single plasma electron, then multiplying that by the electron density. It is assumed that electron collisions are well separated in time and occur only one at a time. Since three-body and higher-order interactions are ignored, a screening prescription (Sec 5.3) is needed to keep the calculations accurate.

We observe that all of the usable expressions for the analytic theory, equations (4.23), (4.21), and (4.22) contain a factor of electron density. This means that they consider only the effect of a single electron in the plasma and multiply their expression by the electron density. It is worth noting that the more general expressions in the relaxation and kinetic theories do contain prescriptions for including multi-electron collisions. But these expressions are generally complicated and have not been implemented yet within analytic calculations.

The validity of this approximation breaks down when three-body or four-body interactions start becoming important. This breakdown occurs when density and, probably more importantly, plasma coupling goes up. This is one of the major advantages of simulation calculations because this effect is included implicitly in the construction of the particle simulations. Figure 15 shows differences in Ly$\alpha$ profiles between simulation (which includes $N$-body collisions automatically), and VCS [48] (which uses a binary-collision approximation).

### *5.8. Impact Approximation*

The impact approximation takes the binary-collision approximation one step further. The electron collisions are assumed to be weak, short, and well separated in time, which results in an autocorrelation function, $C(t)$ in equation (4.3), that decays exponentially. This results in the impact-theory line shapes being Lorentzian. This approximation ignores the transient effects of the collisions and focuses only on the electron broadening at line center.

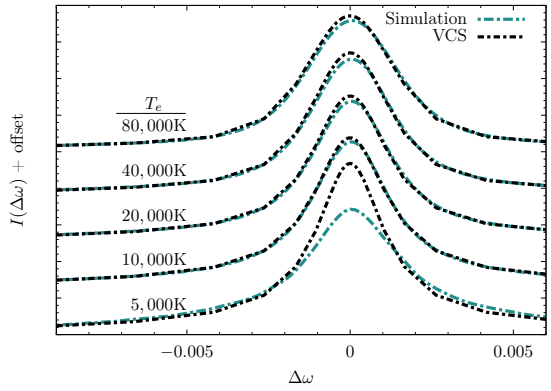


**Figure 15.** Comparison of VCS (which uses the binary-collision approximation) and simulation (which does not) for the Ly$\alpha$ line. VCS and simulation are shown in black and green, respectively. The binary-collision approximation is valid at all temperatures considered here except for the $T_e = 5,000$K.

The impact approximation is the basis of the line-shape theory of Griem [38, 74, 75, 72] and Baranger [76, 25, 44]. Electron-broadened line shapes closely approximate Lorentzians at line center but deviate significantly in the line wing. Figure 16 demonstrates the differences in the profile as a result of using the impact approximation vs fully accounting for the time dependence of the collisions.

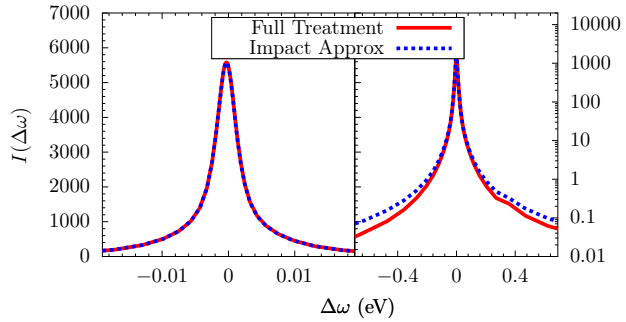


**Figure 16.** Comparison of neutral hydrogen Ly$\alpha$ line shapes with and without using the impact approximation (blue and red respectively). Using the impact approximation results in incorrect wing behavior. The left panel shows the similarities in the core (and is shown in a linear scale), while the right panel shows that the two calculations diverge in the wings (in log scale).

### *5.9. The Approximations used by Different Methods*

We have so far listed approximations used by a variety of line-shape calculations, and the impact that they might have on the line shape. It is clear from the above discussion that each approximation has its own range of validity, and there will be some transition, temperature, or density where that approximation breaks down.

We therefore choose to list which codes employ which approximations in table 1. It is important to note that, so far, no calculation has removed all these approximations

and that some codes will do better at capturing certain physics than others. In this table, we have color-coded the cells, indicating how each code treats a particular type of physics. Calculations that use the approximate form are colored in orange. Those that use the approximate form, but with a correction, are yellow. And those that treat the physics without approximation are in teal. Some of the cells do not contain any text; these indicate that a calculation automatically takes into account the relevant effect without approximation. For example, the $2^{nd}$-order approximation is irrelevant to simulations, so those cells are colored teal without text.

**Table 1.** Table of Common Calculations and the Approximations They Employ. The different cells are color coded according to whether they are using the approximate form (orange), an approximate form with a correction (yellow), or the exact form (teal). Cells that have no text are because that approximation does not apply to that code, and using the exact form is inherently part of that calculation. In the interaction column, "FC" denotes "full-Coulomb" and the addition of "E" denotes that exchange is included.

| | Approximations | | | | | | | |
|---|---|---|---|---|---|---|---|---|
| Refs. | $V_{rp}$ | Density Matrix | Classical/ Quantum | Ion Motion | Exact/ Second Order | Screening | N-body Effects | Electron Dynamics |
| Kepple-Griem[74] | Dipole | Factorized | Classical | Static | $2^{nd}$ | Cutoff | Binary | Impact |
| (VCS) [77] | Dipole | Factorized | Classical | Static | exact | Cutoff | Binary | |
| (MERL) [78] | Dipole | Factorized | Quantum | Static | $2^{nd}$ | Correl | Binary | |
| (TOTAL) [79] | Dipole | Factorized | Quantum | Static | $2^{nd}$-order | Correl | Binary | |
| (PPP) [33] | Dipole | Factorized | Classical | Static | $2^{nd}$-order | Cutoff | Binary | Impact |
| (MELS) [80] | Dipole | Factorized | Classical | Static | $2^{nd}$-order | Cutoff | Binary | Impact |
| (ER Simulation) [30] | Dipole | Factorized | Classical | Dynamic | | Debye | Str-Path | |
| (SimU) [34] | Dipole | Factorized | Classical | Dynamic | | Debye | Str-Path | |
| (Xenomorph) [35] | Dip+Quad | Factorized | Classical | Dynamic | | Debye | Str-Path | |
| (Balrog) [73] | FC + E | Factorized | Quantum | Static | | Debye | Binary | |
| [81] | Dipole | Factorized | Classical | dynamic | $2^{nd}$ | Cutoff | Binary | |
| [55] | FC | Factorized | Quantum | static | $2^{nd}$-order | Cutoff | Binary | |
| [57] | FC | | Quantum | static | $2^{nd}$-order | Debye | Binary | |
| [53] | FC+ E | | Quantum | static | $2^{nd}$-order | Debye | Binary | |
| [22] | FC+E | Factorized | Quantum | static | $2^{nd}$-order | Debye | Binary | |
| [82] | FC | Factorized | Classical | static | $2^{nd}$-order | Debye | Binary | Impact |
| [69] | FC+E | Factorized | Quantum | Static | | None | Binary | Impact |
| [83] | Dipole | Factorized | Classical | Dynamic | | Debye | Str-Path | |
| [28] | Dipole | Factorized | Classical | Dynamic | | N/A | | |
| [29] | Dipole | Factorized | Classical | Dynamic | | N/A | | |
| [84] | Dipole | Factorized | Classical | Static | $2^{nd}$-order | Debye | Str-Path | |
| [85] | Dipole | Factorized | Classical | Static | $2^{nd}$-order | Cutoff | Binary | |

## 6. Future Outlook

There are a couple of aspects that are clear paths forward for simulations and analytic calculations. Simulations are currently limited to the dipole approximation. This means that they are unable to include the red shift from monopole interactions. Therefore, expanding the simulations capability to include a full-Coulomb interaction would be a priority. This is especially important as it has recently been demonstrated that the shift can be a powerful plasma diagnostic [61]. In analytic calculations, now that all-order capabilities have finally been realized, the next step would be to include the effects of 3-or-4-body interactions. Additionally, future analytic calculations might include a more detailed treatment of the nearest neighboring ion on the spectra. In hydrogen, collisions with the nearest ion gives rise to quasi-molecular satellites [See e.g. 86]. Fortunately, the method for doing this is available through the work of Zammit *et al.* [87]

Given the recent impact of quantum electrons shown by Refs [22, 73], quantum effects may need to be included into simulations. One possibility is that the non-locality of plasma electrons could be mocked up using a Gaussian wavepacket. How simulations would include the impact of electron capture [22] is unclear, though three-body recombination is something that can be included in the fully interacting simulations [29].

One aspect that all calculations could look to improve on—except for Gigosos *et al.* [29] and Stambulchik *et al.* [28]—would be a better prescription of screening. At the moment, nearly all line-shape calculations use screening to approximately account for $N$-body interactions that they are neglecting. It is clear from Stambulchik *et al.* [28] that line-shape models that use simple screening approximations do not reproduce line shapes generated with full $N$-body dynamics. Debye screening is the most commonly used screening prescription but is only valid in weakly-coupled plasmas. In strongly coupled plasmas, a different screening prescription would be required to preserve accuracy. Additionally, it is typical to calculate the screening length using only the electrons, ignoring the contribution to the ions. Exactly how to include the ions in the screening is an open debate. Therefore, it is highly desirable to improve screening prescriptions for broader range of plasma conditions.

We mentioned in section 1 that plasma effect also have an effect on the continuum, advancing it to lower energies. For this document, we ignored any discussion about the continuum, but it is modified due to density effects. Models of how the continuum is modified due to the plasma, such as occupation probability [88, 89], extend the continuum to lower energies, and often use a statistical mechanics approach rather than rigorous atomic physics. Treating plasma effects on the continuum is a complex problem that has been largely neglected. Continuum problems are not without their challenges, how to perturb continuum states being one of the principal obstacles.

## 7. Acknowledgements

We would like to thank the many collaborators who have given lots of guidance, feedback and critique over the years: E. Stambulchik, C. Iglesias, S. Alexiou, R.W. Lee, I. Bray, R.C. Mancini, D.E. Winget, M.H. Montgomery, Y. Ralchenko. Without them, this work, which is a culmination of years of effort would not be possible. We would also like to thank Drs. S.B. Hansen and M.A. Schaeuble for providing feedback on the manuscript. Sandia National Laboratories is a multimission laboratory managed

and operated by National Technology and Engineering Solutions of Sandia, LLC., a wholly owned subsidiary of Honeywell International, Inc., for the U.S. Department of Energy's National Nuclear Security Administration under contract DE-NA-00035 25. The work of T.G. and T.N. was performed under a Laboratory Directed Research and Development program at Sandia National Laboratories. The work of M.Z., C.F., and D.K. was carried out under the auspices of the US Department of Energy by Los Alamos National Laboratory under contract No. 89233218CNA000001. P.C. acknowledges support from DOE NNSA Laboratory Residency Graduate Fellowship program support, which is provided under cooperative agreement number DE-NA0003960. The views expressed in the article do not necessarily represent the views of the U.S. Department of Energy or the United States Government.

## A. Derivation of the Fundamental Line-Shape Formula

This section is devoted to deriving the fundamental formula for line shapes, beginning with the formula for the spontaneous radiative decay rate. The rate for spontaneous emission of a photon from an initial state, $i$, to a final state, $f$, is given by the Einstein $A$ coefficient,

$$A_{if} = \frac{\omega^3}{3c^3} |\left\langle i \left| \vec{D} \right| f \right\rangle|^2, \tag{A.1}$$

where $\omega$ is the angular frequency of radiation, which for simplicity we call frequency. Using the absorption coefficient is an equally valid approach and will result in the same expression for the line shape. The emitted power is proportional to the sum of all Einstein $A$ coefficients that contribute to that frequency of radiation,

$$P(\omega) = \frac{4\omega^4 e^2}{3c^3} \sum_{if} \delta(\omega - \omega_{if}) |\left\langle i \left| \vec{D} \right| f \right\rangle|^2 \rho_{ii}, \tag{A.2}$$

where the delta function ensures that only transitions are at the frequency $\omega$ contribute to the power, and $\rho_{ii}$ is the probability that state $i$ is occupied. It is common to separate out the "line-shape" part of the emitted power [27],

$$I(\omega) = \sum_{if} \delta(\omega - \omega_{if}) |\left\langle i \left| \vec{D} \right| f \right\rangle|^2 \rho_{ii}. \tag{A.3}$$

We can express the line-shape formula in terms of an average dipole autocorrelation function, which is the starting point for many line-shape papers. To accomplish this task, we need to re-write this expression as a Laplace transform,

$$\sum_{if} \delta(\omega - \omega_{if}) |\left\langle i \left| \vec{D} \right| f \right\rangle|^2 \rho_{ii} = \frac{1}{\pi} \Re \int_0^\infty dt e^{i\omega t} \sum_{if} e^{-i\omega_{if} t} |\left\langle i \left| \vec{D} \right| f \right\rangle|^2 \rho_{ii}. \tag{A.4}$$

Recognizing that $\omega_{if} = E_i - E_f$, we can write equation (A.4) as

$$\sum_{if} \delta(\omega - \omega_{if}) |\left\langle i \left| \vec{D} \right| f \right\rangle|^2 \rho_{ii} = \frac{1}{\pi} \Re \int_0^\infty dt \; e^{i\omega t} \sum_{if} \left\langle i \left| \vec{D} \right| f \right\rangle e^{iE_f t} \left\langle f \left| \vec{D} \right| i \right\rangle e^{-iE_i t} \rho_{ii}. \tag{A.5}$$

If we define the states $i$ and $f$ to be eigenstates of the Hamiltonian, $H$, then we can replace the energies with $H$. Additionally, we can also write the summation as a trace,

$$I(\omega) = \frac{1}{\pi} \Re \int_0^\infty dt \; e^{i\omega t} Tr \left\{ \vec{D} e^{iHt} \vec{D} e^{-iHt} \rho \right\}. \tag{A.6}$$

We recognize that the quantity $e^{iHt} D e^{-iHt}$ is simply the time evolution of the dipole moment, $D(t)$, according to the Heisenberg picture. Due to the cyclical invariance of the trace, we can also write this equation as

$$I(\omega) = \frac{1}{\pi} \Re \int_0^\infty dt \; e^{i\omega t} Tr \left\{ \vec{D} e^{-iHt} \rho \vec{D} e^{iHt} \right\}, \tag{A.7}$$

which now includes the density matrix in the time evolution. This latter form is convenient for certain types of calculation.

In equation (A.6), we have defined the line shape as being the Laplace transform of the average $\vec{D}\cdot\vec{D}(t)$, which is the dipole autocorrelation function, often referred to as $C(t)$. The average dipole autocorrelation function is

$$C(t) = Tr\left\{\vec{D}\cdot\vec{D}(t)\rho\right\}. \tag{A.8}$$

This result indicates that the line shape is a measure of how much the atom deviates from the dipole moment at the initial time. We expect that the average of fluctuations at long times to average out and this quantity to be zero. At shorter times, however, $C(t)$ is non-zero and describes the radiative behavior of the atom [26].

## B. On the Liouville Notation

We can use the Liouville notation to write the time evolution of the dipole moment in a compact way. The Liouville operator can be used to calculate equations of motion and master equations [90, 91, 92]. The Liouville operator is a superoperator, meaning that it operates on other operators rather than operating on state vectors. The Liouville operator is a shorthand notation for a commutation of an operator—say the dipole moment—with the Hamiltonian,

$$L\vec{D} = [H, \vec{D}] = H\vec{D} - \vec{D}H. \tag{B.1}$$

We can see how the Liouville operator can simplify the notation describing time evolution by differentiating $D(t)$,

$$\begin{aligned}
\frac{d}{dt}\left[e^{iHt}\vec{D}e^{-iHt}\right] &= iHe^{iHt}\vec{D}e^{-iHt} - ie^{iHt}\vec{D}e^{-iHt}H \\
\frac{d}{dt}\vec{D}(t) &= iH\vec{D}(t) - i\vec{D}(t)H \\
\frac{d}{dt}\vec{D}(t) &= iL\vec{D}(t).
\end{aligned} \tag{B.2}$$

This means that we can write the time evolution equivalently as a function of the Liouville operator,

$$\vec{D}(t) = e^{iHt}\vec{D}e^{-iHt} = e^{iLt}\vec{D}. \tag{B.3}$$

This means that the Liouville provides a compact way of writing the fundamental equations, and lends itself to easy algebraic manipulation. For example, performing a Laplace transform becomes quite simple,

$$\int_0^\infty dt\; e^{i\omega t}e^{iLt}\vec{D} = \frac{-i}{\omega + L}\vec{D}. \tag{B.4}$$

A matrix element of the Liouville operator will be a function of four state variables rather than the usual two state variables. Ordinarily, an operator is a function of two states, a bra and a ket,

$$\left\langle i\left|\vec{D}\right|f\right\rangle, \tag{B.5}$$

where $i$ and $f$ are states. According to equation (B.1), the quantity $L\vec{D}$ is also a regular operator that is a function of two states. A given matrix element of $L\vec{D}$ is

defined as

$$\begin{aligned}
\left\langle i\left|L\vec{D}\right|f\right\rangle &= \left\langle i\left|H\vec{D}\right|f\right\rangle - \left\langle i\left|\vec{D}H\right|f\right\rangle \\
&= \sum_m \langle i|H|m\rangle \left\langle m\left|\vec{D}\right|f\right\rangle - \sum_n \left\langle i\left|\vec{D}\right|n\right\rangle \langle n|H|f\rangle \\
&= \sum_{m,n} \left[\langle i|H|m\rangle \delta_{fn} - \delta_{im}\langle n|H|f\rangle\right] \langle m|D|n\rangle \\
&= \sum_{m,n} \langle if|L|mn\rangle \langle m|D|n\rangle \\
\langle if|L|mn\rangle &= \langle i|H|m\rangle \delta_{fn} - \delta_{im}\langle n|H|f\rangle . \qquad \text{(B.6)}
\end{aligned}$$

Representing the Liouville operator as a matrix results in matrices that are much larger than ordinary operators. In an ordinary operator—i.e., non-tetradic—then each state vector is an element in the matrix,

$$D = \begin{bmatrix} D_{11} & D_{12} & D_{13} & \cdots \\ D_{21} & D_{22} & D_{23} & \cdots \\ D_{31} & D_{32} & D_{33} & \cdots \\ \vdots & \vdots & \vdots & \ddots \end{bmatrix}. \qquad \text{(B.7)}$$

However, in the tetradic notation, the $D$ matrix is turned into a vector,

$$D = \begin{bmatrix} D_{11} \\ D_{12} \\ D_{13} \\ \vdots \\ D_{21} \\ D_{22} \\ D_{23} \\ \vdots \end{bmatrix}, \qquad \text{(B.8)}$$

and the Liouville super-operator is defined as a tetradic matrix,

$$LD = \begin{bmatrix} (LD)_{11} \\ (LD)_{12} \\ \vdots \\ (LD)_{21} \\ (LD)_{22} \end{bmatrix} = \begin{bmatrix} L_{11,11} & L_{11,12} & \cdots & L_{11,21} & L_{11,22} & \cdots \\ L_{12,11} & L_{12,12} & \cdots & L_{12,21} & L_{12,22} & \cdots \\ \vdots & & & & & \\ L_{21,11} & L_{21,12} & \cdots & L_{21,21} & L_{21,22} & \cdots \\ L_{22,11} & L_{22,12} & \cdots & L_{22,21} & L_{22,22} & \cdots \end{bmatrix} \begin{bmatrix} D_{11} \\ D_{12} \\ \vdots \\ D_{21} \\ D_{22} \\ \vdots \end{bmatrix}.$$

## C. The $T$-matrix and the Lippmann-Schwinger Equation

Formally, the $T$-matrix is related to a collision amplitude. It is typical to define the total scattering wavefunction at large distances as an incoming plane wave (with momentum $\vec{k}$) plus an outgoing scattered wave

$$\Psi(\vec{r}) \xrightarrow[\vec{r}\to\infty]{} e^{i\vec{k}\cdot\vec{r}} + f(\theta,\varphi)\frac{e^{ikr}}{r}, \qquad \text{(C.1)}$$

where $f(\theta, \phi)$ is the scattering amplitude. This simple picture of scattering is ignoring the wavefunction of the radiator atom. The $T$-matrix is formally related to the scattering amplitude by

$$\langle a\alpha \,|T(E)|\, a\alpha' \rangle = -\frac{2\pi}{m} f_{a\to a'}(\theta, \varphi), \tag{C.2}$$

where $a$ and $a'$ denote atomic states, and $\alpha$ and $\alpha'$ denote perturbing electron states. Due to this relationship, we can therefore use $T$-matrices to directly calculate cross sections.

We can derive a more formal definition for the $T$-matrix; this is through the Lippmann-Schwinger equation. We first define

$$H_0 \,|\phi\rangle = E \,|\phi\rangle \tag{C.3}$$

$$(H_0 + V) \,|\psi\rangle = E \,|\psi\rangle \,. \tag{C.4}$$

We can re-arrange equation (C.4) so that

$$(E - H_0) \,|\psi\rangle = V \,|\psi\rangle \,. \tag{C.5}$$

Now, in the limit that $V$ vanishes, we wish that $|\psi\rangle \to |\phi\rangle$, we can modify this expression that gives us an initial condition,

$$(E - H_0) \,|\psi\rangle = (E - H_0) \,|\phi\rangle + V \,|\psi\rangle \tag{C.6}$$

Then dividing through by $(E - H_0)$, we arrive at the Lippmann-Schwinger equation,

$$|\psi\rangle = |\phi\rangle + \frac{1}{E - H_0} V \,|\psi\rangle \,. \tag{C.7}$$

It is clear that this form is analogous to equation (C.1), though more formally derived.

From this Lippmann-Schwinger equation, we can derive the $T$-matrix. Repeated application of the integral equation in equation (C.7) gives for the second-term on the right-hand side

$$\frac{1}{E - H_0} V \,|\psi\rangle = \frac{1}{E - H_0} \left[ V + V \frac{1}{E - H_0} V + \cdots \right] |\phi\rangle \,. \tag{C.8}$$

The quantity in the square brackets can be written as a Taylor series in one of two equivalent ways

$$\sum_{n=0}^{\infty} V \left[ \frac{1}{E - H_0} V \right]^n = V \frac{1}{1 - (E - H_0)^{-1} V} \tag{C.9}$$

$$\sum_{n=0}^{\infty} \left[ V \frac{1}{E - H_0} \right]^n V = \frac{1}{1 - V(E - H_0)^{-1}} V. \tag{C.10}$$

Therefore, we can write the Lippmann-Schwinger equation as a function of the $T$-matrix

$$|\psi\rangle = |\phi\rangle + \frac{1}{E - H_0} T(E) \,|\phi\rangle \,, \tag{C.11}$$

thus establishing the relationship between the $T$-matrix and the scattering amplitude.

There are a few more relationships that we would like to spell out here, including an integral form of the $T$-matrix. In the above, we can compare equations (C.11) and (C.7), and show that

$$T(E)\,|\phi\rangle = V\,|\psi\rangle\,. \tag{C.12}$$

From this relationship, we can obtain an integral definition of the $T$-matrix, where

$$V\,|\psi\rangle = V\,|\phi\rangle + V\frac{1}{E-H_0}V\,|\psi\rangle\,. \tag{C.13}$$

Then application of equation (C.12), gives us the following integral relationship,

$$T(E)\,|\phi\rangle = V\,|\phi\rangle + V\frac{1}{E-H_0}T(E)\,|\phi\rangle\,. \tag{C.14}$$

We can write the $T$-matrix in another form without the use of integral functions. We can achieve this by manipulating equation (C.7),

$$\begin{aligned}
|\psi\rangle &= |\phi\rangle + \frac{1}{E-H_0}V\,|\psi\rangle \\
(E-H_0)\,|\psi\rangle &= (E-H_0)\,|\phi\rangle + V\,|\psi\rangle \\
(E-H_0-V)\,|\psi\rangle &= (E-H_0-V+V)\,|\phi\rangle \\
|\psi\rangle &= |\phi\rangle + \frac{1}{E-H_0-V}V\,|\phi\rangle\,.
\end{aligned} \tag{C.15}$$

Combining equation (C.15) with equation (C.12), we can write the $T$-matrix as

$$T(E) = V + V\frac{1}{E-H_0-V}V. \tag{C.16}$$

The relationships derived here can be derived by other methods, but we hope that this gives some insight into the related quantities. There are a few more things to discuss here about the $T$-matrix, namely how to evaluate the function $(E-H_0)^{-1}$, the relationship between the $T$-matrix and other relevant matrices, and the relationship of $E$ to the state vectors the $T$-matrix is applied to. Each of these will need its own subsection.

### *C.1. The Green's function*

The operator $(E-H_0)^{-1}$ is often known as the Green's function, the propagator, and the resolvent operator. This operator has a singularity in it, therefore what is often done is to introduce a small imaginary part in the denominator, then take the limit as that small imaginary part goes to zero. In this limit, we obtain real and imaginary parts of the Green's function,

$$\lim_{\eta\to 0}\frac{1}{E+i\eta-H_0} = \frac{\text{p.v.}}{E-H_0} - i\pi\delta(E-H_0), \tag{C.17}$$

where p.v. stands for Cauchy principal value and $\delta()$ is a Dirac delta function. Handling of the Dirac delta function is trivial and there is universal consensus on how to handle it. The real part, the principal value, is more challenging, and there are several different methods for how to treat it.

For the purposes of this section, we assume that the perturber wavefunction can be described with spherical harmonics. We will also work in the momentum representation of the wavefunction.

The evaluation of the principal value and delta function only make sense in the context of an integral. The Green's functions are usually sandwiched between other operators, and resolution of identity will mean that Green's functions will be evaluated with an integral. For example, one way to evaluate a product of operators is to introduce a complete set of states

$$V\frac{1}{E-H_0}V = \sum_a \int dk_\alpha k_\alpha^2 V\left|a\alpha\right\rangle \frac{1}{E-E_a-\frac{1}{2m}k_\alpha^2}\left\langle a\alpha\right|V; \tag{C.18}$$

we can do this because states $|a\alpha\rangle$ are eigenstates of the $H_0$ operator,

$$H_0\left|a\alpha\right\rangle = (E_a+E_\alpha)\left|a\alpha\right\rangle, \tag{C.19}$$

where for free states of the perturbing electron, the energy is defined by the square of its momentum, $E_\alpha = \frac{1}{2m}k_\alpha^2$. If we insert equation (C.17) into our example, then the evaluation of $V[E-H_0]^{-1}V$ becomes

$$\begin{aligned} V\frac{1}{E-H_0}V = & \\ & \sum_a \int dk_\alpha k_\alpha^2 V\left|a\alpha\right\rangle \frac{\text{p.v.}}{E-E_a-\frac{1}{2m}k_\alpha^2}\left\langle a\alpha\right|V \\ & -i\pi\sum_a \int dk_\alpha k_\alpha^2 V\left|a\alpha\right\rangle \delta\left(E-E_a-\frac{1}{2m}k_\alpha^2\right)\left\langle a\alpha\right|V. \end{aligned} \tag{C.20}$$

The second term becomes trivial. If we define a quantity $q$ such that

$$\frac{1}{2m}q^2 = E-E_a. \tag{C.21}$$

Then the integral vanishes except when $k_\alpha = q$. The second term on the right-hand-side of equation (C.20) therefore reduces to

$$-i\pi\sum_a qV\left|aq\right\rangle\left\langle aq\right|V; \quad q=\sqrt{2m(E-E_a)}. \tag{C.22}$$

### *C.1.1. Adding a Term to Remove the Singularity*

This method is used by O'Brien & Hooper [56] and McCarthy & Stelbovics [93], where the property that

$$\int_0^\infty dk_\alpha 2m\frac{1}{q^2-k_\alpha^2} = 0 \tag{C.23}$$

means that the right-hand side can be subtracted from Eq (C.20). The resulting expression for $V\text{p.v.}[E-H_0]^{-1}V$ becomes

$$\begin{aligned} & \sum_a \int dk_\alpha k_\alpha^2 V\left|a\alpha\right\rangle \frac{\text{p.v.}}{E-E_a-\frac{1}{2m}k_\alpha^2}\left\langle a\alpha\right|V \\ & \qquad -\sum_a \int dk_\alpha k_\alpha^2 V\left|aq\right\rangle \frac{\text{p.v.}}{E-E_a-\frac{1}{2m}k_\alpha^2}\left\langle aq\right|Vq^2. \end{aligned} \tag{C.24}$$

The advantage here is that the numerator and denominator go to zero at the same order,

$$\sum_a \int dk_\alpha V \frac{|a\alpha\rangle \langle a\alpha| \, k_\alpha^2 - q^2 \, |aq\rangle \langle aq|}{\frac{1}{2m}(q^2 - k_\alpha^2)} V \quad \text{(C.25)}$$

which means the singularity vanishes and the principal value is no longer needed.

### *C.1.2. Strategic Placement of Quadrature Points*

A quadrature is simply the transformation of an integral into a summation. If we define $J = \int dk f(k)$, then we can approximate it as $J \approx \sum_i w_i f(k_i)$, where the set of $i$ are points in $k$ chosen to accurately represent the integral, and the $w_i$ are the summation weights, usually closely related to some $\Delta k_i$. Therefore, in our example above, we can represent the integral as a summation with weights,

$$\sum_a \int dk_\alpha k_\alpha^2 V \, |a\alpha\rangle \, \frac{\text{p.v.}}{E - E_a - \frac{1}{2m}k_\alpha^2} \langle a\alpha| \, V \Rightarrow \sum_{a,k_i} V \, |a\alpha\rangle \, w(k_i) \, \langle a\alpha| \, V. \quad \text{(C.26)}$$

A very simple method of integration would be to choose weights

$$w(k_i) = k_i^2 \Delta k_i \frac{1}{E - E_a - \frac{1}{2m}k_i^2}, \quad \text{(C.27)}$$

where $\Delta k_i$ is some integration step in the $k_\alpha$ integral. Careful selection of the set of $k_i$, one could use this method to avoid having to integrate over the singularity; this is roughly the method used by Bray & Stelbovics [94].

### *C.1.3. Performing the* p.v. *integral inside a Quadrature rule*

In this method, which is the one used by Gomez *et al.* [22] and Gomez *et al.* [73], we use a quadrature rule. The weights are determined by assuming that the $V$ operator is constant over some $\Delta k$. We then define

$$w(k_i) = \int_{(k_i+k_i-1)/2.}^{(k_i+k_i+1)/2} dk \; k^2 \frac{\text{p.v.}}{\frac{1}{2m}(q^2 - k^2)}, \quad \text{(C.28)}$$

for which analytic solutions exist. For the results, we will use a shorthand, where we assign $a$ to be the lower limit of integration and $b$ to be the upper limit of integration. The resulting weight values are

$$w(k_i) = \frac{k_i^2}{|q|} \begin{cases} \ln\frac{q-b}{q+b} - \ln\frac{q-a}{q+a} & \text{if } q > b \\ \ln\frac{b-q}{q+b} - \ln\frac{a-q}{q+b} & \text{if } q < a \\ \ln\frac{b-q}{q+b} - \ln\frac{q-a}{q+b} & \text{if } a < q < b \\ q\left[\frac{2}{b} - \frac{2}{a}\right] & \text{if } q = 0 \\ 2\left[\arctan(a/|q|) - \arctan(b/|q|)\right] & \text{if } q^2 < 0. \end{cases} \quad \text{(C.29)}$$

*C.1.4. Bilinear form of Green's function*

This is an expression of the Green's function in terms of position [95],

$$\left\langle r \left| \frac{1}{E - H_0} \right| r' \right\rangle. \tag{C.30}$$

This is done by inserting a complete set of states that are solutions of $H_0$,

$$\left\langle r \left| \frac{1}{E - H_0} \right| r' \right\rangle = \int dk dk' \langle r|k\rangle \left\langle k \left| \frac{1}{E - H_0} \right| k' \right\rangle \langle k'|r'\rangle. \tag{C.31}$$

This expression is then written in terms of eigenstates of $H_0$,

$$\left\langle r \left| \frac{1}{E - H_0} \right| r' \right\rangle = \int dk \frac{\phi_k(r)\phi_k^*(r')}{E - E_k + i\eta}. \tag{C.32}$$

This has the advantage of removing the singularity, no longer needing to evaluate the principal value [96].

*C.2. Some useful Relationships: "Reactance" K-matrix and "Scattering" S-matrix*

Now that we have seen that the Green's function has a real and imaginary part, we can take the expression in equation (C.14) and derive the $K$-matrix. We begin with the integral expression for the $T$-matrix,

$$T(E) = V + V\left[\Re G(E) + \Im G(E)\right] T(E)$$

where we have abbreviated the Green's function as $G(E)$. Then, we manipulate the equation as so,

$$\begin{aligned} T(E) &= V + V\left[\Re G(E) + \Im G(E)\right] T(E) \\ \left[1 - V\Re G(E)\right] T(E) &= V + V\Im G(E) T(E) \\ T(E) &= K(E) + K(E)\Im G(E) T(E) \end{aligned}$$

where the K-matrix is equal to

$$\begin{aligned} K(E) &= \frac{1}{1 - V\frac{\text{p.v.}}{E - H_0}} V \\ &= V \frac{1}{1 - \frac{\text{p.v.}}{E - H_0} V}. \end{aligned}$$

Further manipulation of the $T$-matrix equation gives us the following relationship between the $T$-matrix and the $K$-matrix

$$T(E) = \frac{1}{1 + i\pi K(E)\delta(E - H_0)} K(E). \tag{C.33}$$

We can then, with some algebraic manipulations using the $K$-matrix, separate out the real and imaginary parts of the $T$-matrix,

$$\begin{aligned} T(E) = K(E) \frac{1}{1 + \left[\pi\delta(E - H_0)K(E)\right]^2} \\ - i\pi T^\dagger(E)\delta(E - H_0)T(E). \end{aligned} \tag{C.34}$$

The expression for the imaginary part is known as the optical theorem. We write the optical theorem explicitly as

$$\Im T(E) = -\pi T^\dagger(E)\delta(E - H_0)T(E). \tag{C.35}$$

The optical theorem can also be derived from the $S$-matrix and its unitarity condition [46].

The last relationship we want to show is the scattering "S"-matrix, which is defined in terms of a $T$-matrix,

$$S = 1 - 2i\pi\delta(E - H_0)T(E) \tag{C.36}$$

or equivalently in terms of the $K$-matrix

$$S = \frac{1 - i\pi\delta(E - H_0)K(E)}{1 + i\pi\delta(E - H_0)K(E)}. \tag{C.37}$$

It is not difficult to see that $S^{-1} = S^\dagger$. Therefore, this means that the $S$-matrix is unitary operator, meaning that $SS^\dagger = 1$.

*C.3. Relationship of $E$ to the state vectors: On-Shell and Off-Shell $T$-matrices*

When one takes a matrix element of the $T$-matrix,

$$\langle \alpha\mathbf{k}|T(E)|\,\alpha'\mathbf{k}'\rangle\,,$$

we can see that the resulting matrix element is a function of $E$. How that energy, $E$, relates to the states $\alpha\mathbf{k}$ and $\alpha'\mathbf{k}'$ will dictate whether the $T$-matrix is on the energy shell or off the energy shell (or half-on shell). What this means is the when the matrix element is fully on shell, the in and out energies are the same, as is the energy parameter, $E$. For half-on-shell $T$-matrices, the energy is equal to only one of the in or out energies. And for off-shell, $E$ equals neither the in or out energies. These relationships are given here,

$$\text{on shell} \qquad E = E_{\alpha\mathbf{k}} = E_{\alpha'\mathbf{k}'} \tag{C.38}$$

$$\text{half on shell} \qquad \begin{cases} E = E_{\alpha\mathbf{k}} \neq E_{\alpha'\mathbf{k}'} \\ E = E_{\alpha'\mathbf{k}'} \neq E_{\alpha\mathbf{k}} \end{cases} \tag{C.39}$$

$$\text{fully off shell} \qquad E \neq \begin{cases} E_{\alpha\mathbf{k}} \\ E_{\alpha'\mathbf{k}'}. \end{cases} \tag{C.40}$$

The physical interpretation of the half-off shell or fully off shell scenarios is that a non-energy conserving virtual photon is involved to change the energy of either the incoming or outgoing states. However, in the line-shape problem, this can be interpreted as a real (instead of virtual) photon.

## D. The $M$-operator and the Collision $T$-matrix

In the relaxation theory above, Fano [26] expressed the width in terms of Liouville operators, in what he called the (memory) "$M$"-operator. The $M$-operator is defined as

$$M(\omega) = \frac{1}{1 - L_I(\omega - L_0)^{-1}}L_I. \tag{D.1}$$

Calculating matrix elements of $M(\omega)$ is complex because of the enormous size of the matrix, it is therefore more convenient to calculate $M(\omega)$ in smaller, more manageable, chunks. This particular task can be done by expressing $M(\omega)$ in terms of $T$-matrices.

Fano did this, and we will quote the results here. However, the expression for $M(\omega)$ is complicated, and we need to establish some definitions. We have already introduced the $H_0$ operator, which is the non-interacting Hamiltonian that operates on both the atom and perturbing electron; in this section we will use the subscript "$0r$" or "$0l$" to denote whether $H_0$ is operating from the right or left side. Additionally, any variables that have a $^*$ superscript denotes a lower state interaction, which is complex conjugated. $M(\omega)$ is therefore defined in terms of non-tetradic operators

$$M(\omega) = \frac{1}{1 - L_I(\omega - L_0)^{-1}} L_I \tag{D.2}$$

$$\begin{aligned} &= T(\omega + H^*_{0r})\delta_{H^*_{0r},H^*_{0l}} - T^*(H_{0r} - \omega)\delta_{H_{0r},H_{0l}} \\ &+ i\pi\delta(\omega - H_{0l} + H^*_{0r})T(H_{0l})T^*(H^*_{0r}) \\ &+ i\pi\delta(\omega - H_{0r} + H^*_{0l})T(H_{0r})T^*(H^*_{0l}) \\ &+ \frac{1}{2}M_{transient}(\omega). \end{aligned} \tag{D.3}$$

The first term is the upper-state broadening, the second term is the lower-state broadening, terms 3 and 4 are interference terms, and $M_{transient}(\omega)$ are additional terms which represent the transient effects of the collision. $M_{transient}(\omega)$ is defined as

$$\begin{aligned} M_{transient} &= \text{p.v.}\frac{T(H_{0l})T^*(H_{0l} - \omega) - T(H_{0r})T^*(H_{0r} - \omega)}{H_{0l} - \omega - H^*_{0r}} \\ &-\text{p.v.}\frac{T(H^*_{0l} + \omega)T^*(H_{0l}) - T(H^*_{0r} + \omega)T^*(H^*_{0r})}{\omega - H_{0r} + H^*_{0l}} \\ &+\frac{T(H^*_{0l} + \omega)T^*(H_{0l}) - T(H^*_{0r} + \omega)T^*(H^*_{0r})}{H^*_{0l} - H^*_{0r}} \\ &-\frac{T(H_{0l})T^*(H_{0l} - \omega) - T(H_{0r})T^*(H_{0r} - \omega)}{H_{0l} - H_{0r}} \\ &+\frac{g(H_{0l}) - g(H_{0r})}{H_{0l} - H_{0r}} + \frac{g(H^*_{0l} + \omega) - g(H^*_{0r} + \omega)}{H^*_{0l} - H^*_{0r}} \\ &-\frac{g(H_{0l}) - g(H_{0r} + \omega)}{H_{0l} - \omega - H^*_{0r}} - \frac{g(H^*_{0l} + \omega) - g(H_{0r})}{H^*_{0l} + \omega - H^*_{0r}}, \end{aligned} \tag{D.4}$$

where

$$g(E) = \frac{1}{2\pi i}\int_{-\infty}^{\infty} dE' \frac{\text{p.v.}}{E' - E} T(E')T^*(E' - \omega). \tag{D.5}$$

The transient broadening term, $M_{transient}(\omega)$, is zero if the $T$-matrices are independent of the energy argument. This means that in a large portion of cases, $M_{transient}(\omega)$ is likely to be negligible, but this has never been tested/verified.

## References


[1] Hubeny I and Mihalas D 2014 *Theory of Stellar Atmospheres*

[2] Winget D E, Hansen C J, Liebert J, van Horn H M, Fontaine G, Nather R E, Kepler S O and Lamb D Q 1987 *Astrophysical Journal Lett* **315** L77

[3] Bailey J E, Nagayama T, Loisel G P, Rochau G A, Blancard C, Colgan J, Cosse P, Faussurier G, Fontes C J, Gilleron F, Golovkin I, Hansen S B, Iglesias C A, Kilcrease D P, Macfarlane J J, Mancini R C, Nahar S N, Orban C, Pain J C, Pradhan A K, Sherrill M and Wilson B G 2015 *Nature* **517** 56–59

[4] Nagayama T, Bailey J E, Mancini R C, Iglesias C A, Hansen S B, Blancard C, Chung H K, Colgan J, Cosse P, Faussurier G, Florido R, Fontes C J, Gilleron F, Golovkin I E, Kilcrease D P, Loisel G, MacFarlane J J, Pain J C, Rochau G A, Sherrill M E and Lee R W 2016 *High Energy Density Physics* **20** 17–22

[5] Gomez T A, Cho P B, Hubeny I, Hobbs B, Dunlap B H, Fontes C J, Kilcrease D P, Nagayama T, Montgomery M H and Winget D E 2021 The Sensitivity of White Dwarf Atmosphere Models to the Broadening of the Ly$\alpha$ line in prep

[6] Gomez T, Nagayama T, Kilcrease D, Hansen S, Montgomery M and Winget D 2018 Influence of Projection Operator on Oxygen Line Shapes and its effect on Rosseland-Mean Opacity in Stellar Interiors *American Astronomical Society Meeting Abstracts #231* (*American Astronomical Society Meeting Abstracts* vol 231) p 452.02

[7] Basu S and Antia H M 2008 *Physics Reports* **457** 217–283

[8] Wiese W L, Kelleher D E and Paquette D R 1972 *Phys. Rev. A* **6** 1132–1153

[9] Iglesias C A 2016 *High Energy Density Physics* **18** 14–19

[10] Condon E U and Shortley G H 1935 *The Theory of Atomic Spectra*

[11] Bethe H A and Salpeter E E 1957 *Quantum Mechanics of One- and Two-Electron Atoms* (New York: Academic Press)

[12] Cowan R D 1981 *The Theory of Atomic Structure and Spectra* (Los Alamos Series in Basic and Applied Sciences, Berkeley: University of California Press, 1981)

[13] Heitler W 1954 *Quantum Theory of Radiation* (Dover Publications, inc)

[14] Starrett C E and Saumon D 2013 *Phys. Rev. E* **87** 013104

[15] Belkhiri M and Poirier M 2013 *High Energy Density Physics* **9** 609–617

[16] Belkhiri M and Fontes C J 2016 *Journal of Physics B Atomic Molecular Physics* **49** 175002

[17] Hussey T, Dufty J W and Hooper C F 1975 *Phys. Rev. A* **12** 1084–1093

[18] Abdallah J, Clark R E H, Csanak G and Cowan R D 1988 Los Alamos National Laboratory, Los Alamos Manual No. LA 11436-M-I

[19] Fontes C J, Zhang H L, Abdallah J J, Clark R E H, Kilcrease D P, Colgan J, Cunningham R T, Hakel P, Magee N H and Sherrill M E 2015 *Journal of Physics B Atomic Molecular Physics* **48** 144014

[20] Sampson D H, Zhang H L and Fontes C J 2009 *Physics Reports* **477** 111–214

[21] Gu M F 2008 *Canadian Journal of Physics* **86** 675–689

[22] Gomez T A, Nagayama T, Fontes C J, Kilcrease D P, Hansen S B, Zammit M C, Fursa D V, Kadyrov A S and Bray I 2020 *Phys. Rev. Lett.* **124** 055003

[23] Fano U 1957 *Reviews of Modern Physics* **29** 74–93

[24] Anderson P W 1949 *Physical Review* **76** 647–661

[25] Baranger M 1958 *Physical Review* **111** 494–504

[26] Fano U 1963 *Physical Review* **131** 259–268

[27] Griem H R 1974 *Spectral line broadening by plasmas* (New York, Academic Press, Inc. (Pure and Applied Physics. Volume 39), 1974. 421 p.)

[28] Stambulchik E, Fisher D V, Maron Y, Griem H R and Alexiou S 2007 *High Energy Density Physics* **3** 272–277

[29] Gigosos M A, González-Herrero D, Lara N, Florido R, Calisti A, Ferri S and Talin B 2018 *Phys. Rev. E* **98** 033307

[30] Gigosos M A, Cardenoso V and Torres F 1986 *Journal of Physics B Atomic Molecular Physics* **19** 3027–3033

[31] Cho P B, Gomez T A, Montgomery M H, Fitz Allen M, Hobbs B, Hubeny I and E W D 2021 Simulations of Stark-Broadened Hydrogen Balmer Line Shapes for DA White Dwarf Synthetic Spectra submitted

[32] 2021 `https://plasma-gate.weizmann.ac.il/slsp/`

[33] Calisti A, Khelfaoui F, Stamm R, Talin B and Lee R W 1990 *Phys. Rev. A* **42** 5433–5440

[34] Stambulchik E and Maron Y 2006 *J. Quant. Spec. Radiat. Transf.* **99** 730–749

[35] Gomez T A, Nagayama T, Kilcrease D P, Montgomery M H and Winget D E 2016 *Phys. Rev. A* **94** 022501

[36] Djurović S, Ćirišan M, Demura A V, Demchenko G V, Nikolić D, Gigosos M A and González M Á 2009 *Phys. Rev. E* **79** 046402

[37] Rosato J, Marandet Y and Stamm R 2020 *J. Quant. Spec. Radiat. Transf.* **249** 107002

[38] Griem H R, Kolb A C and Shen K Y 1959 *Physical Review* **116** 4–16

[39] Baranger M and Mozer B 1959 *Physical Review* **115** 521–525

[40] Hooper C J 1968 *Physical Review* **165** 215–222

[41] Tighe R J and Hooper C F J 1977 *Phys. Rev. A* **15** 1773–1779

[42] Iglesias C A, Dewitt H E, Lebowitz J L, MacGowan D and Hubbard W B 1985 *Phys. Rev. A* **31** 1698–1702

[43] Boercker D B, Iglesias C A and Dufty J W 1987 *Phys. Rev. A* **36** 2254–2264

[44] Baranger M 1958 *Physical Review* **112** 855–865

[45] Kolb A C and Griem H 1958 *Physical Review* **111** 514–521

[46] Lippmann B A and Schwinger J 1950 *Physical Review* **79** 469–480

[47] Smith E W 1968 *Physical Review* **166** 102–113

[48] Smith E W, Cooper J and Vidal C R 1969 *Physical Review* **185** 140–151

[49] Bogoliubov N N 1946 *Journal of Experimental and Theoretical Physics* **16** 691–702

[50] Kirkwood J G 1946 *The Journal of Chemical Physics* **14** 180–201

[51] Kirkwood J G 1947 *The Journal of Chemical Physics* **15** 72–76

[52] Born M and Green H S 1946 *Proceedings of the Royal Society of London A: Mathematical, P hysical and Engineering Sciences* **188** 10–18 ISSN 0080-4630

[53] Gomez T A, Nagayama T, Kilcrease D P, Montgomery M H and Winget D E 2018 *Phys. Rev. A* **98** 012505

[54] Griffiths D J 1995 *Introduction to Quantum Mechanics*

[55] Woltz L A and Hooper Jr C F 1984 *Phys. Rev. A* **30** 468–473

[56] O'Brien J T and Hooper Jr C F 1974 *J. Quant. Spec. Radiat. Transf.* **14** 479–496

[57] Junkel G C, Gunderson M A, Hooper Jr C F and Haynes Jr D A 2000 *Phys. Rev. E* **62** 5584–5593

[58] Saemann A, Eidmann K, Golovkin I E, Mancini R C, Andersson E, Förster E and Witte K 1999 *Phys. Rev. Lett.* **82** 4843–4846

[59] Dervieux V, Loupias B, Baton S, Lecherbourg L, Glize K, Rousseaux C, Reverdin C, Gremillet L, Blancard C, Silvert V, Pain J C, Brown C R D, Allan P, Hill M P, Hoarty D J and Renaudin P 2015 *High Energy Density Physics* **16** 12–17

[60] Stillman C R, Nilson P M, Ivancic S T, Golovkin I E, Mileham C, Begishev I A and Froula D H 2017 *Phys. Rev. E* **95** 063204

[61] Kraus B F, Gao L, Hill K W, Bitter M, Efthimion P C, Gomez T A, Moreau A, Hollinger R, Wang S, Song H, Rocca J J and Mancini R C 2021 *Phys. Rev. Lett.* **127** 205001

[62] Smith E W, Vidal C R and Cooper J 1969 *J. Res. Natl. Bur. Stand. A, Phys Chem.* **73A(4)** 389–404

[63] Griem H R, Iglesias C A and Boercker D B 1991 *Phys. Rev. A* **44** 5318–5319

[64] Boercker D B and Iglesias C A 1984 *Phys. Rev. A* **30** 2771–2774

[65] Iglesias C A 2021 *High Energy Density Physics* **38** 100921

[66] Bohr N 1920 *Zeitschrift fur Physik* **2** 423–469

[67] Alexiou S and Ralchenko Y 1994 *Phys. Rev. A* **49** 3086–3088

[68] Glenzer S and Kunze H J 1996 *Phys. Rev. A* **53** 2225–2229

[69] Griem H R, Ralchenko Y V and Bray I 1997 *Phys. Rev. E* **56** 7186–7192

[70] Alexiou S and Lee R W 2006 *J. Quant. Spec. Radiat. Transf.* **99** 10–20

[71] Lee R W 1979 *Journal of Physics B Atomic Molecular Physics* **12** 1129–1143

[72] Griem H R, Blaha M and Kepple P C 1979 *Phys. Rev. A* **19** 2421–2432

[73] Gomez T A, Nagayama T, Cho P, C Z M, Fontes C J, Kilcrease D P, Bray I, Hubeny I, Dunlap B, Montgomery M H and Winget D E 2021 All-Order Full-Coulomb Quantum Spectral Line-Shape Claculations submitted

[74] Kepple P and Griem H R 1968 *Physical Review* **173** 317–325

[75] Kepple P C 1972 *Phys. Rev. A* **6** 1–9

[76] Baranger M 1958 *Physical Review* **111** 481–493

[77] Vidal C R, Cooper J and Smith E W 1973 *ApJS* **25** 37

[78] Woltz L A and Hooper Jr C F 1988 *Phys. Rev. A* **38** 4766–4771

[79] Lee R W 1988 *J. Quant. Spec. Radiat. Transf.* **40** 561–568

[80] Iglesias C A and Sonnad V 2010 *High Energy Density Physics* **6** 399–405

[81] Stehle C and Jacquemot S 1993 *A&A* **271** 348

[82] Alexiou S and Poquérusse A 2005 *Phys. Rev. E* **72** 046404

[83] Alexiou S 2005 *Phys. Rev. E* **71** 066403

[84] Stamm R, Smith E W and Talin B 1984 *Phys. Rev. A* **30** 2039–2046

[85] Rosato J, Capes H and Stamm R 2012 *Phys. Rev. E* **86** 046407

[86] Allard N F, Drira I, Gerbaldi M, Kielkopf J and Spielfiedel A 1998 *A&A* **335** 1124–1129

[87] Zammit M C, Fursa D V and Bray I 2014 *Phys. Rev. A* **90** 022711

[88] Dappen W, Anderson L and Mihalas D 1987 *Astrophysical Journal* **319** 195

[89] Hummer D G and Mihalas D 1988 *Astrophysical Journal* **331** 794

[90] Zwanzig R 1960 *J. Comp. Physics* **33** 1338–1341

[91] Zwanzig R 1964 *Physica* **30** 1109–1123

[92] Zwanzig R 2001 *Nonequilibrium Statistical Mechanics* (OUP USA) ISBN 9780195140187 URL `https://books.google.com/books?id=oKPmCwAAQBAJ`

[93] McCarthy I E and Stelbovics A T 1983 *Phys. Rev. A* **28** 2693–2707

[94] Bray I and Stelbovics A T 1992 *Phys. Rev. A* **46** 6995–7011

[95] Mott N, Massey H and Massey H 1965 *The Theory of Atomic Collisions* The International Series of Monographs on Physics (Clarendon Press) URL `https://books.google.com/books?id=xUcwAAAAIAAJ`

[96] Bray A W, Abdurakhmanov I B, Kadyrov A S, Fursa D V and Bray I 2015 *Computer Physics Communications* **196** 276–279